Damping mechanisms and order-to-chaos transition in the warm rotating ^{163}Er nucleus

S. Leoni,[1] G. Benzoni,[1] A. Bracco,[1] N. Blasi,[1] F. Camera,[1] C. Grassi,[1] P. Mason,[1] B. Million,[1] A. Paleni,[1] M. Pignanelli,[1] E. Vigezzi,[1] O. Wieland,[1] M. Matsuo,[2] T. Døssing,[3] B. Herskind,[3] G. B. Hagemann,[3] J. Wilson,[3] A. Maj,[4] M. Kmiecik,[4] G. Lo Bianco,[5] C. M. Petrache,[5] M. Castoldi,[6] A. Zucchiatti,[6] G. de Angelis,[7] D. R. Napoli,[7] P. Bednarczyk,[4,8] and D. Curien[8]

[1]*Dipartimento di Fisica, Universitá di Milano and INFN Sez. Milano, Via Celoria 16, I-20133 Milano, Italy*

[2]*Graduate School of Science and Technology, Niigata University, Niigata 950-2181, Japan*

[3]*The Niels Bohr Institute, Blegdamsvej 15-17, DK-2100 Copenhagen, Denmark*

[4]*The Niewodniczanski Institute of Nuclear Physics, Polish Academy of Sciences, PL-31-342 Krakow, Poland*

[5]*Dipartimento di Fisica, Universitá di Camerino and INFN Sez. Perugia, Italy*

[6]*INFN Sez. Genova, Genova, Italy*

[7]*Laboratori Nazionali di Legnaro, Viale dell'Universitá 2, Legnaro (PD), Italy*

[8]*Institut de Recherches Subatomiques, 23 rue du Loess, Bôite Postale 28, F-67037 Strasbourg, France*

(Received 9 May 2005; published 28 September 2005)

The γ decay in the quasicontinuum is used to study the order-to-chaos transition in the thermally excited ^{163}Er nucleus. The experimental analysis is performed on high-statistics EUROBALL data, focusing on the spin region $I \approx (20\text{–}40)\,\hbar$, and internal excitation energy up of $\approx$2.5 MeV. The results are compared to cranked shell model calculations for this nucleus, taking into account the dependence on the K quantum number. Two main topics are investigated. First, the validity of the selection rules associated with the K quantum number are studied as a function of the internal energy U above yrast. K-selection rules are found to be obeyed in the decay along discrete unresolved rotational bands up to $U \approx 1.2$ MeV, whereas in the interval $U \approx 1.2\text{–}2.5$ MeV, where the order-to-chaos transition is expected to take place, selection rules are found to be only partially valid. Second, the line-shape analysis of γ-γ coincidence spectra provides a direct experimental measurement of the rotational and compound damping widths ($\Gamma_{\rm rot}$ and Γ_μ), yielding values of 200 and 20 keV, respectively, in good agreement with theory.

DOI: 10.1103/PhysRevC.72.034307 PACS number(s): 21.10.Re, 21.60.Ka, 23.20.Lv, 27.20.+q

I. INTRODUCTION

The transition between order and chaos in a quantum mechanical system is a fascinating subject that is currently investigated in different research fields. The atomic nucleus is one of the best examples of a finite many-body quantum system for which the interplay between collective and single-particle degrees of freedom can be used to probe the gradual evolution of the system toward a chaotic regime.

For deformed rare-earth nuclei, the order-to-chaos transition should take place at internal excitation energies U somewhere between 0.5 and 7 MeV. The upper limit, 7 MeV, stems from numerous studies of neutron resonances at low spins, which behave in a fully chaotic way, both with respect to level spacings and strength distributions [1]. The lower limit is established by studies of level spacing distributions of states belonging to rotational bands [2], showing that the nucleus behaves as an ordered system at excitation energies above yrast up to about 0.5 MeV. Also, at these low excitation energies, the rotational bands can in a meaningful way be assigned quantum numbers of quasiparticle excitations of a rotating field [3].

At excitation energies larger than about 0.5 MeV above the yrast band, it becomes increasingly difficult to resolve rotational bands. However, in recent years, the region corresponding to values of U up to 2–3 MeV has been investigated for a variety of nuclei, covering different mass regions, deformations, and intrinsic configurations [4]. This provides an opportunity to access precisely the excitation energy region where one expects that the order-to-chaos transition takes place. The experimental analysis has shown that the majority of γ rays emitted in heavy-ion fusion reactions leading to deformed nuclei are of rotational nature. They are associated with a lifetime typical of strongly collective transitions [5] and produce γ-γ coincidence spectra characterized by a typical ridge-valley structure [4]. Such a landscape carries information both on the decay along discrete rotational bands at relatively low excitation energies above yrast (ridges) and on the more excited strongly interacting bands (valley), corresponding to states of typical excitation energies 1 to 2 MeV above yrast. At each angular momentum, the high level density and the interaction among levels give rise to a fragmented decay-out from each state. This leads to spectra that contain numerous weak γ transitions and are appropriately named *quasicontinuum* spectra. The occurrence of many weak transitions and of a fragmented decay may be a sign of an order-to-chaos transition, which can be investigated by analyzing such quasicontinuum distributions [6,7].

Theoretically, the development of cranked shell model (CSM) calculations, which combine the cranked Nilsson mean-field and a residual surface delta two-body interaction (SDI) [8], has provided a microscopic description of nuclear levels and $E2$ transitions in the thermally excited nucleus, making it possible to study in more detail the properties of rapidly rotating nuclei with internal energies up to a few MeV above yrast. In particular, it has been possible to study in detail the interplay of *compound nucleus damping* and *rotational damping* within the same model. The level density rapidly increases as a function of the internal excitation energy U.

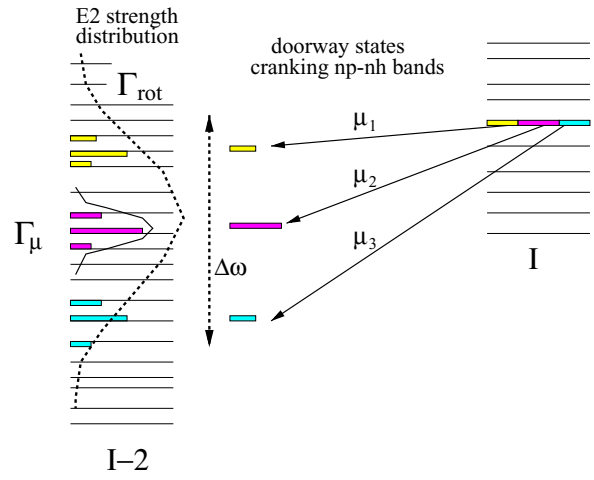

FIG. 1. (Color online) Schematic illustration of the fragmentation of the rotational $E2$ strength from a state at spin I to a number of final states at spin $(I-2)$, as a consequence of the complex nature of the compound nucleus states. In the figure, the μ_i's are *np-nh* unperturbed bands, which are mixed to form a state at spin I. The dispersion $\Delta\omega$ in rotational frequency from spin I to spin $(I-2)$ arises from the different response of each unperturbed band to the rotation. (Adapted from Ref. [12].)

As a consequence, the low-lying rotational bands corresponding to a few particle-hole excitations in the deformed mean field gradually mix via the residual two-body interaction, acquiring a width Γ_μ, named the *compound nucleus damping width*. This leads to a nuclear level spacing distribution that, around $U \approx 2.5-3$ MeV, approaches the one predicted by the Gaussian orthogonal ensemble (GOE), typical of chaotic systems [9,10]. The complex nature of the compound nucleus states has consequences on the rotational motion, since each level on which the rotational bands are built is an admixture of *np-nh* configurations, each one reacting differently to both the Coriolis and centrifugal forces. As a result, the quadrupole γ transitions become *damped*: The decay from a given initial state at spin I acquires a distribution of final states all at spin $(I-2)$, whose FWHM is the *rotational damping width* $\Gamma_{\rm rot}$ [11]. As schematically illustrated in Fig. 1, the $E2$ strength function reflects both the compound and rotational damping mechanisms: whereas the overall profile is determined by $\Gamma_{\rm rot}$, the fine structure, which keeps memory of the rotational correlation in the *np-nh* unperturbed bands, is characterized by Γ_μ. The study of rotational damping can, therefore, shed light on the order-to-chaos transition in the atomic nucleus, since it not only relates to excitation energy regions where such a transition is expected to take place but also makes it possible to obtain estimates for the two damping widths $\Gamma_{\rm rot}$ and Γ_μ, which are determined by the nature of the compound nucleus states.

With increasing internal energy U the calculated $E2$ strength from a given initial state gradually fragments over several final states. A quantitative estimate of this fragmentation is provided by the branching number [8] $n_b(\alpha) = 1/\Sigma_\beta S^2_{\alpha\to\beta}$, where $S_{\alpha\to\beta}$ denotes the normalized rotational transition strength from the level α at angular momentum I to the level β at angular momentum $(I-2)$. The onset of damping can then be defined by the condition $n_b > 2$, which leads to internal energies U of $\approx$1 MeV. This strongly limits the number of levels forming discrete rotational bands, which is generally found to be of the order of 20–40 at most, for each spin value.

In this paper we present an extensive review of the results obtained from a data set on ^{163}Er on which two different techniques, namely the statistical fluctuation [13] and the spectral shape analysis method [14], have been used to investigate in detail the quasicontinuum γ-decay populating states up to $I \approx 40\hbar$ and excitation energy extending up to $U \approx 4$ MeV above yrast. The interpretation of the experimental results will be based, in both cases, on the same (CSM) calculations of Ref. [15], thereby providing a consistent overall picture of the thermally excited rotational motion.

The experimental analysis presented here is based on a high-statistics data set, taken with the EUROBALL array. We have performed a detailed study of the γ-decay flow for selected configurations, associated with high and low values of the K quantum number (the projection of aligned nucleonic angular momentum on the symmetry axis), as discussed in Sec. II.

First, the transition between order and chaos in the excited ^{163}Er nucleus is discussed in Sec. III A in terms of the violation of selection rules associated with the K quantum number, as a function of internal energy U. The analysis is made by comparing the γ-decay flows feeding low-K and high-K discrete bands in terms of statistical fluctuations of the counts collected in the corresponding γ-γ coincidence spectra. In Sec. III B we will present a direct experimental measurement of the rotational and compound damping widths $\Gamma_{\rm rot}$ and Γ_μ in the spin region $I \approx (30–40)\,\hbar$. The first quantity has been studied experimentally at higher spins with a different technique [16], and the latter has only been measured indirectly [17]. The analysis technique is based on the study of the line shape of the quasicontinuum ridge-valley structure observed in γ-γ coincidence spectra. The method makes use of an analytic function that takes into account the complex nature of the $B(E2)$ strength distribution, carrying information on both $\Gamma_{\rm rot}$ and Γ_μ, as shown in Fig. 1.

II. EXPERIMENT

The experiment was performed using the EUROBALL array [18,19] at the IReS Laboratory (France), employing the reaction ^{18}O + ^{150}Nd, at $E_{\rm beam} = 87$ and 93 MeV. The ^{150}Nd target was made of a stack of two thin foils for a total thickness of 740 μg/cm^2 and the corresponding maximum angular momentum reached in the reaction has been calculated to be $40\hbar$ and $45\hbar$, for the two different bombarding energies. Energy-dependent time gates on the Ge time signals were used to suppress neutron-induced background, resulting in a total of $\approx 3\times10^9$ events of triple and higher Ge folds, with ^{162,163}Er as the main evaporation residua. The excitation energy of the most intensely populated bands of ^{163}Er is shown as a function of spin in Fig. 2, for (a) positive parity and (b) negative-parity states, relative to a rigid rotor. In the figure, the labels A and B (E and F) refer to the signature partners positive-parity (negative-parity) bands with low-K quantum number ($K = 5/2$) and represent in fact the yrast bands for each I^π configuration. In addition, K2, K4, and K1 refer to the most

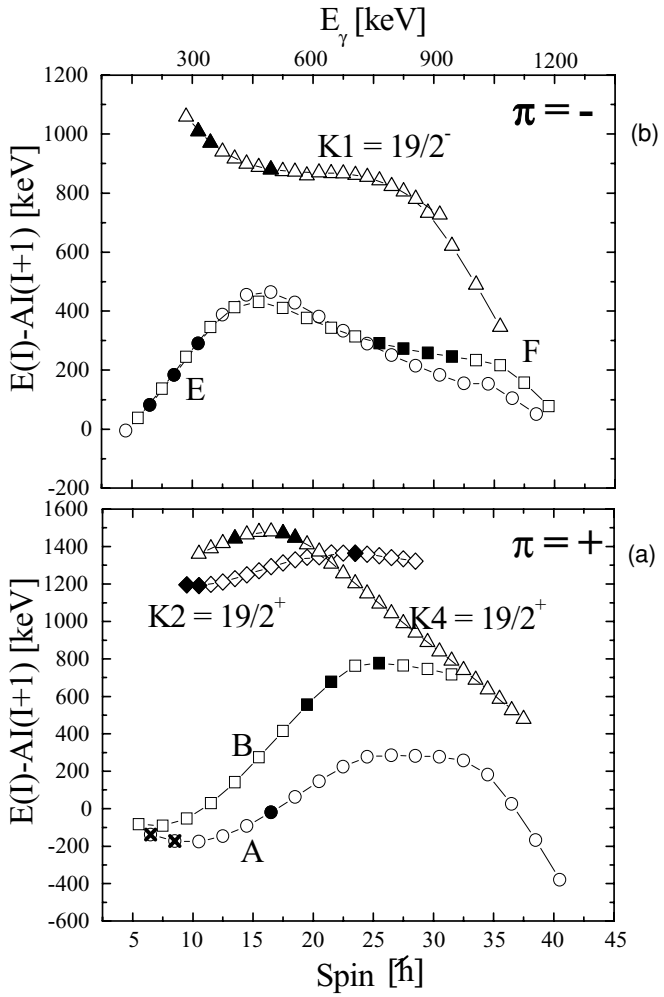

FIG. 2. Excitation energy versus spin of the most strongly populated bands of ^{163}Er, relative to a rigid reference with dynamic moment of inertia $J^{(2)} = 63.6\,\mathrm{MeV}^{-1}\,\hbar^2$. The upper scale of panel (b) refers to the corresponding γ-ray energy E_γ. Panel (a) refers to positive-parity bands, whereas panel (b) to negative-parity bands. The gates used to construct the 2D spectra in coincidence with the different intrinsic configurations are indicated by filled symbols; the transitions of band A used to construct the matrix collecting the total decay flow of ^{163}Er are marked by crosses.

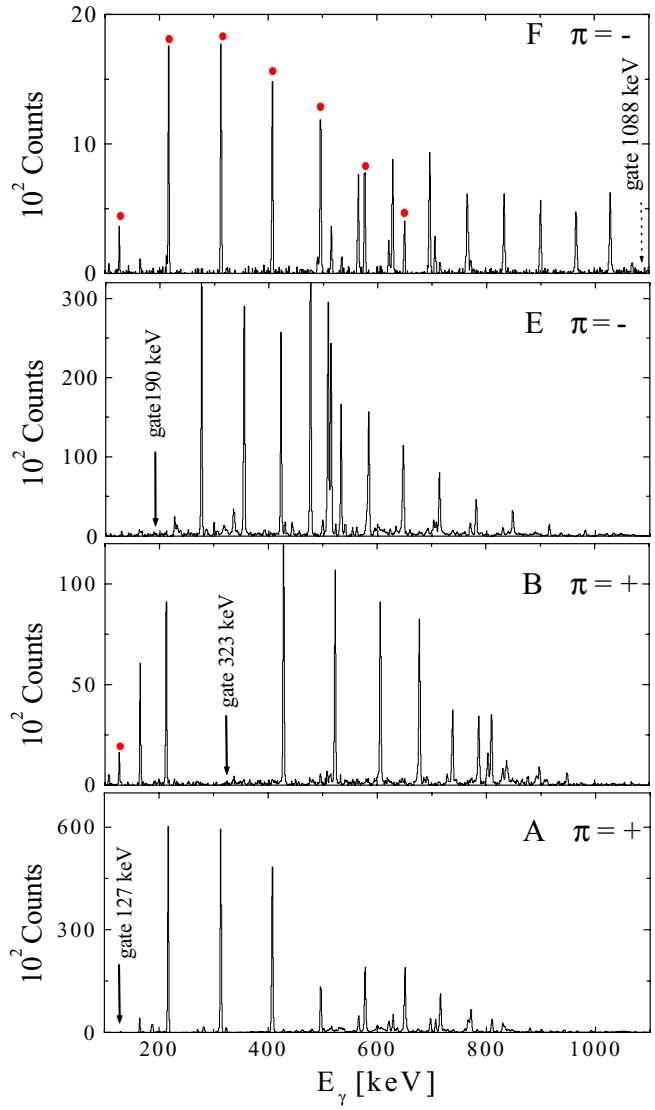

FIG. 3. (Color online) Double-gated spectra of the most intense low-K bands of ^{163}Er, labeled according to Ref. [20]. The spectra have been obtained by setting the additional gate, shown by arrows in the figure, on the corresponding 2D gate-selected matrix and subtracting the gate-related background. Transitions marked by circles occur in band A, to which the specific configuration finally decays.

intensely populated positive- and negative-parity bands with high-K quantum number ($K = 19/2$), following the notation of Ref. [20]. The collected data have been sorted into a number of two-dimensional (2D) matrices in coincidence with specific γ transitions of the ^{163}Er nucleus. In particular, the matrix collecting the entire decay flow of ^{163}Er (named *total*) has been constructed by gating on the two cleanest low-spin transitions of energies 127 and 217 keV, marked by crosses in Fig. 2(a). In addition, seven $E_{\gamma_1} \times E_{\gamma_2}$ spectra in coincidence with transitions belonging to the low-K and high-K bands have been sorted, using the gates marked by filled symbols in Figs. 2(a) and 2(b). In the case of the positive-parity high-K states, since K2 interacts with K4 at $I \approx 21.5\hbar$, single gating conditions are not sufficient to separate the feeding of K2 from the feeding of K4, resulting in gated spectra that contain contribution from both positive-parity states. Each 2D gated spectrum has then been corrected by the corresponding 2D background, obtained by setting narrow gates around the peaks. It should also be noticed that the limited number of gating transitions here used to select a specific intrinsic configuration is a consequence of the difficulty in finding clean gating conditions for the ^{163}Er nucleus. This differs from a previous work reported in Ref. [21], where the use of the BGO Inner Ball resulted in a better selection of the nuclear configurations.

Figures 3 and 4 show examples of one-dimensional spectra corresponding to low-K and high-K bands, respectively. Each spectrum is obtained by setting an additional gate, indicated by an arrow in each figure, on the 2D matrix in coincidence with the specific intrinsic configuration, and subtracting the gate-related background. In Fig. 3, peaks marked by filled circles indicate transitions belonging to band A, to which the

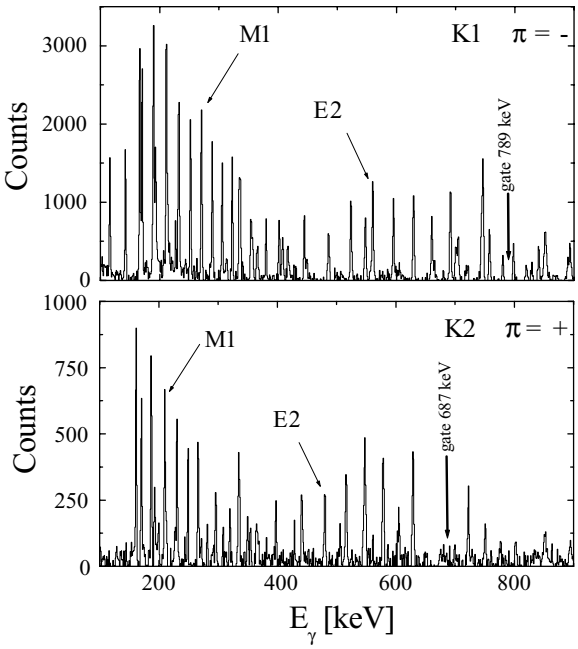

FIG. 4. Double-gated spectra of the most intense high-K bands of ^{163}Er, labeled according to Ref. [20]. The spectra have been obtained by setting the additional gate, shown by arrows in the figure, on the corresponding 2D gate-selected matrix and subtracting the gate-related background. The groups of $M1$ and $E2$ transitions, characteristic of the high-K band structure are indicated by arrows.

specific configuration finally decays. The decay into band A is particularly evident in the F spectrum, as a consequence of the use of gating conditions at rather high spins. In contrast, no transitions from band A are present in the spectrum of configuration E, since the additional 190-keV gate is placed at the bottom of this band ($9/2^- \rightarrow 5/2^-$). In the case of the high-K spectra of Fig. 4, the sequences of in-band $E2$ transitions and $M1$ crossing transitions characteristic of high-K structures are evident. This is clearly visible also in the case of the K2 band, for which the additional gate has been placed above the crossing with the K4 band, to uniquely select contributions from K2. It should also be noticed that in both K1 and K2 spectra no peaks from the yrast band A are present, since both structures finally decay to an isomeric state with half-life $\tau_{1/2} = 0.58\mu s$ [20], outside the electronic range of acquisition.

For the purposes of the analysis discussed in Sec. III all known peak-peak and peak-background coincidences have been subtracted from each 2D spectrum, using the Radware software [22]. In addition, the separately gated matrices have also been added together in one *low-K* (A + B + E + F) and one *high-K* (K1 + K2 + K4) matrix. Figure 5 (left column) shows examples of 60-keV-wide cuts perpendicular to the E_{γ_1}-E_{γ_2} diagonal, in the *total*, *low-K*, and *high-K* γ-γ matrices, at the average transition energy $(E_{\gamma 1} + E_{\gamma 2})/2 = 900$ keV, corresponding to $I = 30\hbar$. The data show clearly the *ridge-valley* structure typical of quasicontinuum spectra of rotational nuclei, with a separation between the two most inner ridges equal to $8\hbar^2/J^{(2)}$, with $J^{(2)}$ being the dynamical moment of inertia of the bands. In particular, although the rather sharp ridges are due to the strong rotational correlations

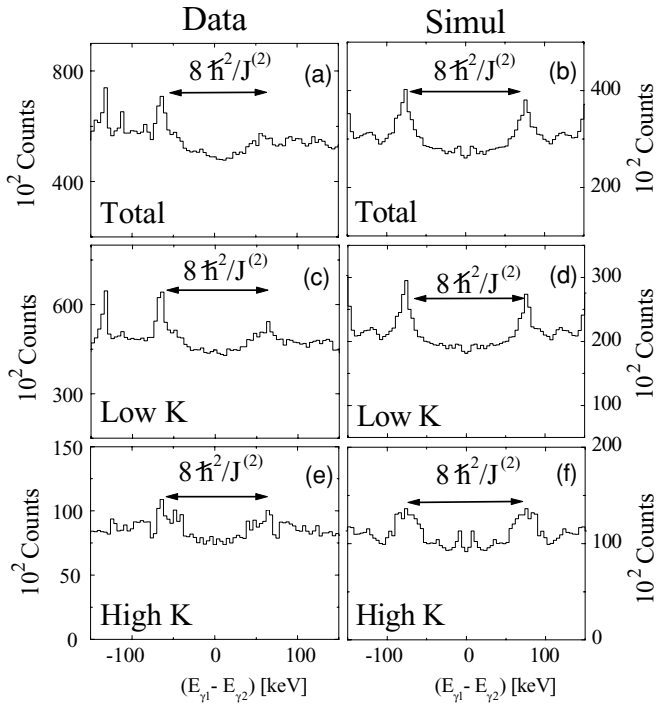

FIG. 5. 60-keV-wide projections perpendicular to the $E_{\gamma_1} = E_{\gamma_2}$ diagonal of experimental and simulated 2D spectra of ^{163}Er (left and right panels, respectively), at the average transition energy $\langle E_\gamma \rangle = 900$ keV. The spectra collect either the total γ-decay flow (a and b) or the γ decay in coincidence with low-K (c and d) or high-K (e and f) configurations. In the simulation, a state is defined as low K (high K) if $K \leqslant 8$ ($K > 8$). The ridge-valley structure typical of rotational nuclei is seen in all spectra, with a separation between the two most inner ridges equal to $8\hbar^2/J^{(2)}$, as indicated by the arrows. The reduced intensity observed in the $E_{\gamma_1} \geqslant E_{\gamma_2}$ region of the spectra is mostly due to the subtraction of all discrete lines known from the level scheme, in the case of the experimental data, and of the yrast and first excited bands, in the case of the simulation. (Adapted from Ref. [13].)

associated with the decay along discrete rotational bands up to $\approx$1 MeV excitation energy above yrast, the rather smooth central valley at $E_{\gamma 1} = E_{\gamma 2}$ mostly collects contributions from the more excited region of strongly interacting bands (rotational damping regime). The asymmetry observed in the intensity of the spectra is due to the discrete line subtraction, which, in this case, is performed only for $E_{\gamma 1} \geqslant E_{\gamma 2}$. The right-hand side of Fig. 5 shows, for comparison, corresponding spectra obtained by the Monte Carlo simulation calculations of the γ-decay cascades [23] discussed in Appendix A.

III. ANALYSIS OF QUASICONTINUUM SPECTRA

In the Past decade, considerable progress has been made in the experimental study of the thermally excited rotational motion mainly as a result of the development of two different techniques: (i) the statistical analysis of the fluctuations of counts in γ-γ matrices [6,24] and (ii) the analysis of the line shape of quasicontinuum γ-γ spectra [12,14]. With these two methods it is possible to perform a quantitative analysis of quasicontinuum spectra populated by the γ decay of the warm rotating

nucleus, providing detailed information on the various quantities entering into the description of the rotational motion at finite temperature (e.g., the number of decay paths followed by the nucleus along the decay and the rotational damping width).

The two different techniques are applied in the following sections to the ^{163}Er data sorted in γ-γ matrices by selecting the decay flow from low-K and high-K structures, as discussed in Sec. II. In particular, the statistical analysis of the spectra, presented in Sec. III A, will make it possible to investigate experimentally the validity of the selection rules on the K quantum number with increasing internal energy U. In addition, the line-shape analysis technique, discussed in Sec. III B, will provide direct experimental estimates of the rotational and compound damping widths $\Gamma_{\rm rot}$ and Γ_{μ}.

Since the two methods rely strongly on a detailed analysis of quasicontinuum distributions, the use of Monte Carlo simulations of the γ-decay cascades is important to sharpen the comparison between experimental data and model predictions [23]. Therefore, the interpretation of the experimental results from both methods will be based on the analysis of simulated γ-γ spectra that are treated with the same tools used for real data. As discussed in detail in Appendix A, the simulated spectra are produced by realistic simulations of the γ-decay flow, produced by the Monte Carlo code MONTESTELLA, based on microscopically calculated energy levels and $E2$ transition probabilities for the specific ^{163}Er nucleus [15].

A. Statistical analysis of γ-γ spectra: violation of the K quantum number with excitation energy

In this paper we relate the question of K-quantum-number violation in excited states to the study of the transition between ordered and chaotic motion in nuclei, caused by the residual interaction and the high level density. In fact, for an ordered system a complete set of single-particle quantum numbers can be defined for each given state, resulting in selection rules on the associated electromagnetic transitions. In contrast, in a chaotic regime, owing to the complex nature of every state, no precise definition of quantum numbers (besides energy, spin, and parity) is possible and selection rules lose their validity [25].

In this context, the investigation of the validity of the selection rules with increasing internal energy U can be used to probe experimentally the gradual transition from order to chaos (which is theoretically expected to take place at $U \approx 2.5$ MeV [9]), giving access to regions where more conventional studies based on level statistics are hard to perform, because of the rapidly increasing level density of interacting configurations. (For a recent study in this direction see Ref. [7].)

In the case of the ^{163}Er nucleus, we have used two experimental observables to determine the validity of the K quantum number at increasing internal energy: the number $N_{\rm path}^{(2)}$ of decay paths measured in coincidence with low-K/high-K discrete bands and the r correlation coefficient [6,24]. A path $i \equiv (i_1, i_2)$ represents a given pair of coincident $E2$ transitions $(E_{\gamma i1}, E_{\gamma i2})$ in a given region of the γ-γ plane. The number $N_{\rm path}^{(2)}$ of paths is defined as the weighted average $1/(\sum_i W_i^2)$, where W_i is the probability to follow path i. Note that in practice $N_{\rm path}^{(2)}$ is affected by the relative population probability and strictly corresponds to the actual number of paths only when all paths are equiprobable, namely when $W_i = 1/N_{\rm path}^{(2)}$. It is found that the number of paths depends on both the level density and the rotational damping width [6]. By selecting two-dimensional energy intervals along the ridge (valley) structure of the γ-γ spectrum the number of paths corresponding to discrete rotational bands (strongly interacting bands) can be estimated, as explained in Sec. III A1.

The correlation coefficient r measures the similarity of two spectra $M(A)$ and $M(B)$, gated by transitions belonging to two different bands A and B. Denoting by $W_i(A)$ and $W_i(B)$ the probability to follow path i when the gates are imposed we define the correlation coefficient as

$$r(A, B) = \frac{\sum_i W_i(A) W_i(B)}{\sqrt{[\sum_i W_i(A)^2][\sum_i W_i(B)^2]}}, \qquad (1)$$

which measures the degree of sharing between decay paths through different sets of states and therefore the extent to which selection rules are obeyed during the decay. Both $N_{\rm path}^{(2)}$ and r can be obtained by a statistical analysis of γ-γ coincidence spectra using the expressions (2) and (5), given later in this section [6,24].

In the following we present experimental results from the fluctuations and covariance analysis on the *total*, *low-K*, and *high-K* γ-γ gated matrices of the ^{163}Er nucleus [13], which was already studied in a previous experiment [21]. In the present case we carry out a complete investigation of the quasicontinuum spectrum up to $\approx$3 MeV of internal energy. The experimental data are also compared with results from similar statistical analysis on simulated γ-γ matrices obtained using the Monte Carlo code based on CSM calculations for the specific nucleus [15], as discussed in Appendix A. The use of the simulation is particularly crucial in the case of the analysis of the valley region, which is populated by transitions coming from the warmest part of the decay where rotational damping dominates. In fact, in such a case it is important to know the different regions of level densities spanned by the γ decay of the excited rotating nucleus, and this can be done by a simulation of the γ-decay flow from the residual nucleus entry distribution down to the yrast line [4].

1. Fluctuation analysis

The fluctuations of counts in each channel of the 2D matrices, expressed as variance and covariance, can be evaluated by the program STATFIT and stored into 2D spectra [6].

From the fluctuation spectra it is possible to extract the effective number of decay paths eventually feeding into the gate-selected band. In fact, because each rotational E_γ cascade on average contributes one count in each $\frac{4\hbar^2}{J^{(2)}}$ interval, the number of decay paths $N_{\rm path}^{(2)}$ (defined as before) corresponding to pairs of γ transitions with energies lying in a chosen $\frac{4\hbar^2}{J^{(2)}} \times \frac{4\hbar^2}{J^{(2)}}$ region can be measured using the simple expression [6]

$$N_{\rm path}^{(2)} = \frac{N_{\rm eve}}{\frac{\mu_2}{\mu_1} - 1} \times P^{(2)}, \qquad (2)$$

where $N_{\rm eve}$ is the number of events, and μ_1 and μ_2 are the first and second moments of the distribution of counts evaluated over the sector $\frac{4\hbar^2}{J^{(2)}} \times \frac{4\hbar^2}{J^{(2)}}$ (corresponding to 60 keV $\times$ 60 keV

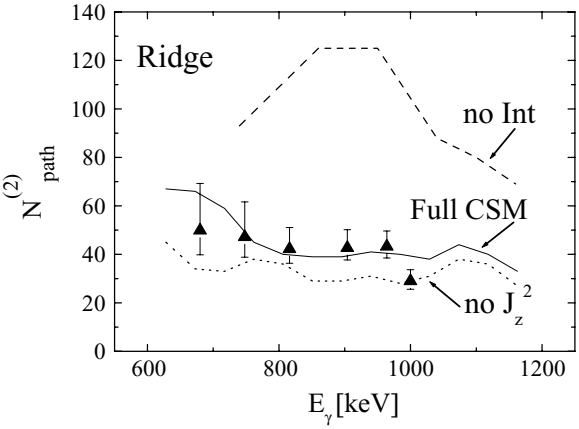

FIG. 6. The experimental total number of discrete paths populating the ridge structure of ^{163}Er (symbols) and the prediction from the CSM of Ref. [15] (solid line). For comparison we also show calculations in which no J_z^2 term (dotted line) or no residual interaction (dashed line) is included in the cranking Hamiltonian.

intervals for rare-earth nuclei around ^{163}Er). In this expression the superscript $^{(2)}$ indicates that the extraction of the number of paths is based on first and second moments; the $P^{(2)}$ factor corrects for the finite resolution of the detector system [6].

In the present analysis we have first evaluated the total number of discrete rotational bands by studying the first ridge of the 2D *total* matrix of ^{163}Er. The experimental results are shown by symbols in Fig. 6, in comparison with the predictions from different types of CSM calculations for the specific nucleus (cf. Appendix A). A total of ≈45 discrete rotational bands at low internal energies is found to exist in the nucleus ^{163}Er, and this is in good agreement with the CSM calculations of Ref. [15], including both the residual interaction and an additional J_z^2 term representing the effect of the K quantum number on the rotational energy (solid line). As shown in the figure, calculations without the residual interaction (dashed line) lead to ridge structures populated by a much larger number of discrete bands, since no fragmentation of the $E2$ strength out of a given state would take place. In contrast, calculations ignoring the J_z^2 term (dotted line) slightly underestimate the total number of paths, since no high-K structures are produced.

The results of the fluctuation analysis on γ-γ matrices gated by specific bands are shown in Fig. 7, for both ridge and valley structures [Figs. 7(a) and 7(b), respectively]. From the analysis of the first ridge, it is found that the number of paths leading to each of the four low-K (A, B, E, and F) and of the three high-K (K1, K2, and K4) configurations is, on average, ≈10. Several of these paths may lead to more than one configuration and this effect can be estimated through the additivity formula [24]

$$\frac{1}{N^{(2)}_{\rm path}} = \sum_i \frac{f_i^2}{N^{(2)}_{{\rm path},i}} \sum_{i\neq j} \frac{r(i,j) f_i f_j}{\sqrt{N^{(2)}_{{\rm path},i} N^{(2)}_{{\rm path},j}}}. \qquad (3)$$

In this expression $N^{(2)}_{{\rm path},i}$ is the number of paths associated with configuration i of relative intensity f_i (in average found to be ≈10); $r(i,j)$ denotes instead the correlation coefficient (experimentally determined in the next section),

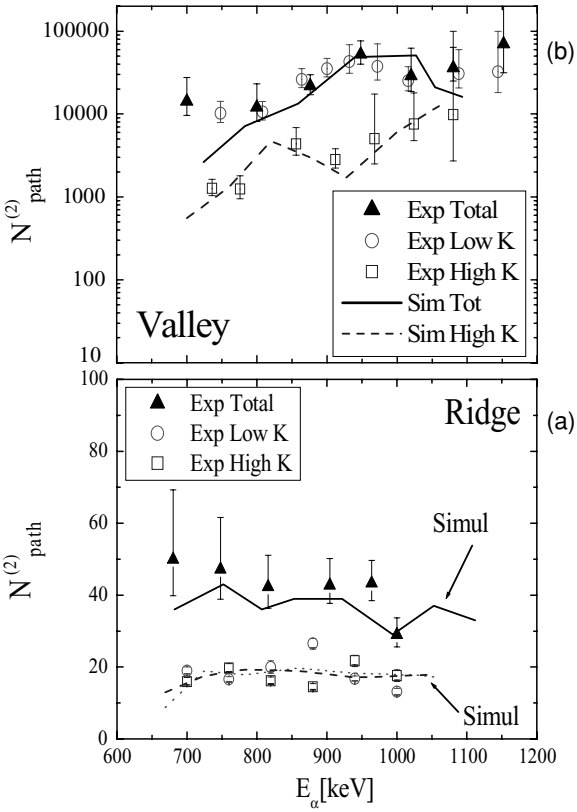

FIG. 7. (a) The number of decay paths extracted from the fluctuation analysis of the ridge structure of ^{163}Er. The open circles (squares) refer to the number of rotational bands populating the first ridge of γ-γ matrices gated by low-K (high-K) configurations; the filled triangles give the number of discrete paths obtained from the total matrix. The corresponding values for simulated spectra are shown by dotted, dashed, and full lines (low K, high K, and total, respectively). (b) The effective number of paths among strongly interacting bands obtained from the fluctuation analysis of the valley region is shown by open circles (squares) for low-K (high-K) gated spectra; the filled triangles show the results obtained from the total γ-γ matrix. The dashed and solid lines give the results for total and high-K cascades, as obtained from simulated spectra. (Adapted from Ref. [13].)

which measures the fraction of paths in common between the two configurations i and j. The results for the total number of low-K and high-K paths are shown in the bottom panel of Fig. 7 by open circles and squares, respectively, and correspond to a total of ≈20 paths, both for low-K and high-K states. In the same figure we report again the total number of bands in the ^{163}Er nucleus (filled triangles as in Fig. 6), in comparison with the number of paths extracted from the fluctuation analysis of the first ridge of the total simulated γ-γ matrix (solid line), as discussed in Appendix A. It is found that the analysis of the total simulated spectra reproduces well the experimental data, being also in accordance with the full CSM calculations shown in Fig. 6. This confirms that the nucleus ^{163}Er contains about 45 discrete bands at low internal energies (≈half of them of high-K character), before damping sets in. It is worth noticing that this is higher than the typical 20 to 25 discrete bands obtained for other nuclei of the rare-earth region (as for

example ^{164,167,168}Yb [6,24]), as a consequence of the presence of the additional 20 high-K bands, which do not exist at such low energies in other nuclei.

The number of paths obtained from the experimental analysis of the valley region, shown in the top panel of Fig. 7, is instead found to depend significantly on the nuclear configuration. In fact, a clear difference in the measured number of paths between low-K and high-K gated spectra is seen up to $E_\gamma \leqslant 1$ MeV, corresponding to spin $I \approx 34\hbar$ and $U \approx 1.5$–2 MeV, being the number of paths in the valley spectra gated by high-K bands almost 10 times smaller than that of low-K bands. Since the valley region is populated by transitions from the regime of strongly interacting bands, such a result indicates that the high-K and low-K states do not mix together in the region of rotational damping. The experimental findings are well reproduced by a similar analysis performed on simulated spectra (shown by lines in the figure), constructed by requiring the same gating conditions on high-K ($K > 8$) and low-K ($K \leqslant 8$) configurations. As discussed in Appendix A, at this excitation energy, not only is the level density for high-K states $\approx$3 times lower than for the low-K ones [15] (cf. Fig. 15), but also the rotational damping width is about reduced 30% for high-K states, as shown both experimentally and theoretically (cf. Appendix B) [14]. Since both the level density and the rotational damping width enter as quadratic terms in a schematic evaluation of the number of paths [6], this roughly explains the factor of 10 separating the number of high-K and low-K gated paths. It should also be noticed that at the highest transition energies studied here, the number of low-K and high-K states approach each other, both in the data and in the simulation, thus indicating a weakening of selection rules on the K quantum number with increasing rotational frequency and internal excitation energy. This should occur at γ-transition energies above 1 MeV, corresponding roughly to angular momenta above $34\hbar$ and energies above yrast typically around 1.5 MeV. This onset of K mixing is found in the calculations to set in at $\approx$1.5 MeV above yrast [15].

2. Covariance analysis

A better understanding of the mixing of states with different K quantum numbers can be obtained by studying the correlations between the fluctuations of the spectra gated on specific low-K and high-K bands. These correlations are expressed by the covariance of counts, defined as

$$\mu_{2,\mathrm{cov}}(A, B) = \frac{1}{N_{\mathrm{ch}}} \sum_j [M_j(A) - \tilde{M}_j(A)][(M_j(B) - \tilde{M}_j(B)], \tag{4}$$

where $M(A)$ and $M(B)$ refer to spectra gated by transitions from two different bands, A and B, and $\tilde{M}$ denotes an average spectrum (which in our case is obtained by the routine STATFIT as a numerical, smoothed third-order approximation to the 2D spectrum) [24]. As in the case of the fluctuation analysis, the sum is over a region spanning N_{ch} channels in a two-dimensional $\frac{4\hbar^2}{\mathcal{J}^{(2)}} \times \frac{4\hbar^2}{\mathcal{J}^{(2)}}$ window. To determine the degree of correlation between the two spectra, the correlation coefficient $r(A, B)$ is calculated:

$$r(A, B) = \frac{\mu_{2,\mathrm{cov}}(A, B)}{\sqrt{[\mu_2(A) - \tilde{\mu}_1(A)][\mu_2(B) - \tilde{\mu}_1(B)]}}, \tag{5}$$

where μ_2 denotes the second moment defined for the same region, related to the expression for the covariance by $\mu_2(A) = \mu_{2,\mathrm{cov}}(A, A)$. The first moment $\tilde{\mu}_1$ is the average of M over the region N_{ch}. The subtraction of the first moments in the denominator of Eq. (5) corrects for the contribution to μ_2 from counting statistics.

The power of the covariance technique is illustrated in Fig. 8, where we show projections perpendicular to the $E_{\gamma_1} = E_{\gamma_2}$ axis of μ_1 (left panels), μ_2 (central panels), and $\mu_{2,\mathrm{cov}}$ spectra obtained from experimental γ-γ matrices of ^{163}Er, gated by different type of structures (explicitly given in each panel). The projections are all taken at the average transition energy $\langle E_\gamma \rangle = 960$ keV, corresponding to $I \approx 32\hbar$. As one can see, the ridge structure is enhanced in the μ_2 fluctuation

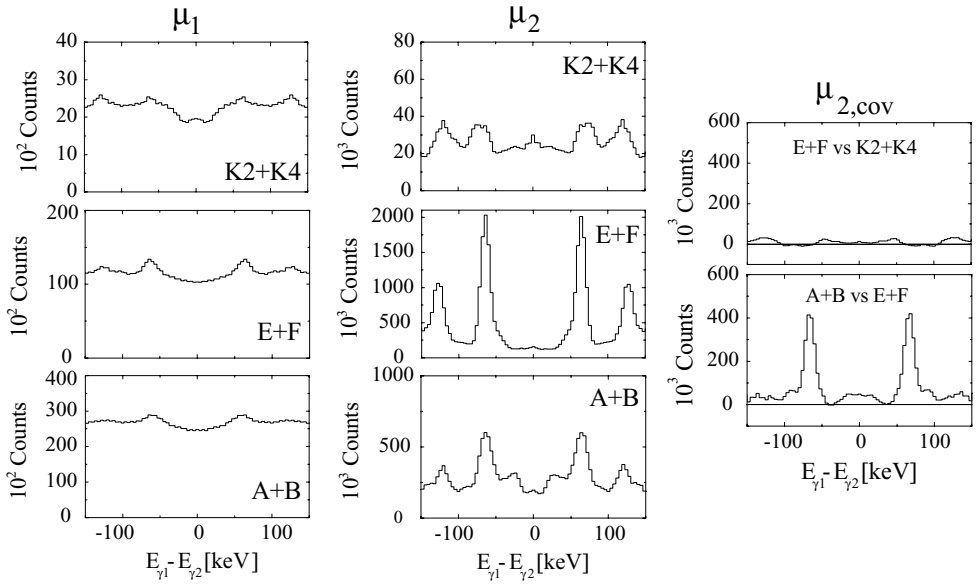

FIG. 8. Spectra of μ_1 (left) and μ_2 (middle) obtained from *experimental* γ-γ coincidence matrices gated by three different types of structures (named in each panel). The spectra have been obtained by projecting the $E_{\gamma_1} \times E_{\gamma_2}$ spectra perpendicularly to the $E_{\gamma_1} = E_{\gamma_2}$ diagonal, with a width of 60 keV and an average transition energy $(E_{\gamma_1} + E_{\gamma_2})/2 = 960$ keV. The right part of the figure shows the covariance between pairs of gated spectra, also evaluated in two dimensions before projection.

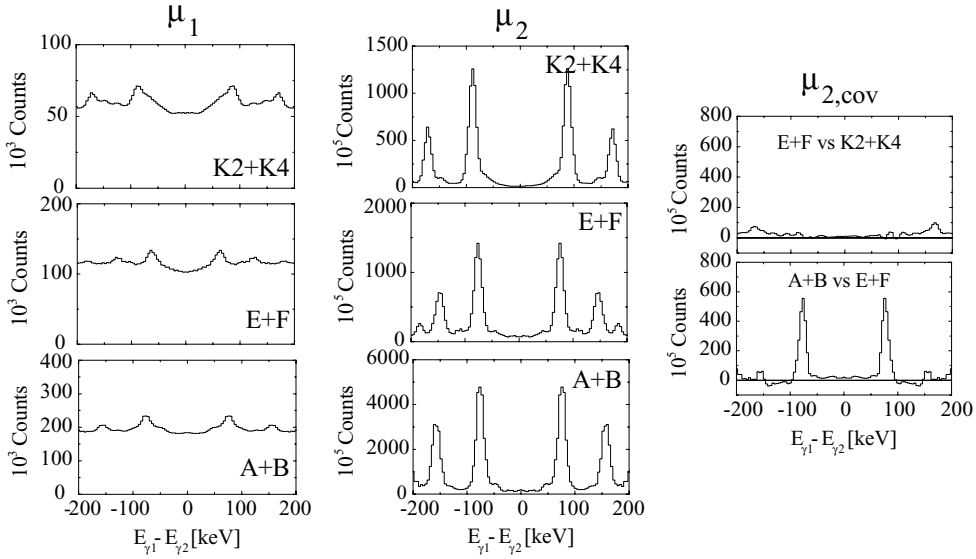

FIG. 9. Spectra of μ_1 (left) and μ_2 (middle) obtained from *simulated* γ-γ coincidence matrices gated by the three different type of structures (named in each panel). The spectra have been obtained by projecting the $E_{\gamma 1} \times E_{\gamma 2}$ spectra perpendicularly to the $E_{\gamma 1} = E_{\gamma 2}$ diagonal, with a width of 60 keV and an average transition energy $(E_{\gamma 1} + E_{\gamma 2})/2 = 960$ keV. The right part of the figure shows the covariance between pairs of gated spectra, also evaluated in two dimensions before projection.

spectra as compared to the original average distribution of counts exhibited by the μ_1 spectrum, even after the removal of all known discrete bands. Such an enhancement, which is less visible in the μ_2 high-K spectrum owing to the lower number of counts in the corresponding μ_1 distribution, confirms the rather low number of discrete regular bands measured by the fluctuation analysis of the ridges, discussed in Sec. III A (cf. Fig. 7). A clear difference is observed in the $\mu_{2,\mathrm{cov}}$ covariance spectra (right panels) in the case of low-K versus low-K as compared to low-K versus high-K combinations. In fact, although in the first case a pronounced ridge structure is observed, in the latter one a rather flat and close to zero distribution is found. This observation indicates that very little correlations are expected among discrete rotational bands characterized by a large difference in the K quantum number.

Figure 9 shows similar projections on the μ_1, μ_2, and $\mu_{2,\mathrm{cov}}$ spectra obtained from simulated γ-γ matrices of ^{163}Er, requiring the same gating conditions as used for the data. Also in this case, very intense ridge structures are observed in the μ_2 spectra, regardless of the selection on K, even more pronounced than in the data, particularly for the high-K spectra. This is related to the discrete line subtraction, which in the case of the simulation is limited to the low-K A, B, E, and F yrast and corresponding first excited bands only, as already discussed in connection with Fig. 5. This implies, in particular, more intense ridge structures in the μ_1 and μ_2 high-K spectra since they include the overall population of high-K states, at variance from the corresponding experimental data from which all known discrete high-K bands have been removed. One should notice, however, that the presence in the simulation of the most strongly populated high-K bands does not affect significantly the results from the fluctuation and covariance analysis, owing to the low intensity of these high-K structures. Similarly to the data, the $\mu_{2,\mathrm{cov}}$ covariance spectra (right panels) show a clear difference between low-K versus low-K and low-K versus high-K combinations, suggesting strong correlations between configurations with similar K quantum number, and almost no mixing between bands with large differences in K, in the excitation energy region probed by the ridges.

The average values of the r coefficient obtained from the analysis of the ridge and valley structures of the experimental and simulated spectra of ^{163}Er, presented in Figs. 8 and 9, are shown by symbols and solid lines in Fig. 10. In the figure, the covariance from the ridge (valley) analysis are presented in the bottom (top) panels, for combinations of low-K versus low-K (left) and low-K versus high-K (right) configurations.

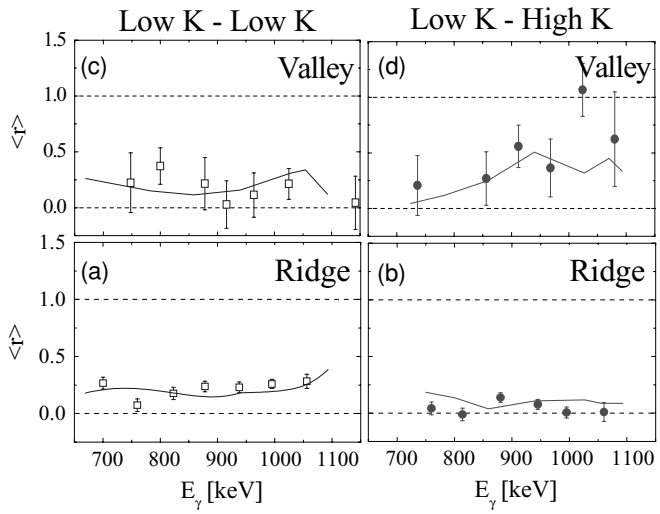

FIG. 10. The results of the covariance analysis on ridge (bottom panels) and valley (top panels) structures of ^{163}Er. Panels (a) and (c) show by open squares the correlation coefficient r obtained experimentally by averaging over pairs of γ-γ spectra gated by low-K configurations; the correlation coefficient obtained from the experimental analysis of the *low-K* versus the *high-K* matrices is shown by filled circles in panels (b) and (d). The theoretical values, as obtained from the covariance analysis of simulated spectra, are represented by solid lines in all the panels; the dashed lines indicate the two extreme limits for full mixing (1) and no mixing (0). (Adapted from Ref. [13].)

In each panel the dashed lines indicate the two opposite limits expected in the case of complete conservation of selection rules ($r = 0$) and of a compound nucleus regime ($r = 1$): As one can see, in all cases good agreement is found between data and simulations. In the case of the ridge analysis, r is found to be of the order of 0.2 for configurations with similar low-K values [Fig. 10(a)], and this can be explained by the fact that at most one or two $E1$ transitions cool the nucleus from the excited unresolved bands below ≈1 MeV of thermal energy, as discussed in Ref. [13]. Such a modest cross talk between regular rotational bands is even more hindered among low-K and high-K states, as testified by the ≈0 correlation coefficients shown in Fig. 10(b), which is a consequence of the flat and ≈0 distributions observed in the covariance spectra (shown in Figs. 8 and 9). This means that there are basically no cross-transitions between the ≈20 bands feeding high-K states and the ≈20 bands feeding low-K states.

For the valley fluctuations, the correlation coefficient is still of the order of 0.2 for low-K versus low-K matrices, thus indicating similar probabilities for $E1$ crossings as in the case of the ridge analysis. In contrast, the r coefficient is found to increase with increasing E_γ in the case of low K versus high K, in accordance with the gradual approach observed in the number of paths for the valley region gated by low-K and high-K bands, shown in Fig. 7(b). Both results suggest a weakening of selection rules associated with the K quantum number with increasing rotational frequency and internal excitation energy, which produce a gradual mixing of low- and high-K configurations. The present analysis is in good agreement with the theoretical predictions from the band-mixing model on ^{163}Er discussed in Appendix A, for which the limit of strong K mixing is only achieve above 2.5 MeV internal excitation energy.

B. Line-shape analysis of γ-γ spectra: direct measurement of the damping widths $\Gamma_{\rm rot}$ and Γ_μ

A line-shape analysis technique has been recently developed to directly extract the rotational and compound damping widths $\Gamma_{\rm rot}$ and Γ_μ from the data [12,14]. The method follows the theoretical observation that the $E2$ strength function, namely the distribution of $E2$ transition energies, reflects both the rotational and compound damping width, through the doorway mechanism schematically illustrated in Fig. 1: Although the overall profile is determined by $\Gamma_{\rm rot}$, fine structures are characterized by Γ_μ, which carries rotational correlations in the unperturbed *np-nh* bands. As a consequence, direct information on both the rotational and compound damping width can be obtained by studying the strength function for two consecutive $E2$ γ decays, $(I + 2) \rightarrow I \rightarrow (I - 2)$, which characterizes the shape of the first ridge as well as the central valley in 2D γ-coincidence spectra (cf. Fig. 5) [12]. Figure 11(a) shows the 2D $E2$ strength calculated for ^{163}Er at spin $I = 40\hbar$-$41\hbar$ for the levels 11–100, for each I^π (corresponding to the average internal energy $\langle U \rangle \approx 1.4$ MeV), therefore excluding the contributions from the ≈45 discrete low-lying rotational bands (cf. Fig. 6). As one can see, the calculated $E2$ strength distribution shows a complex structure with a characteristic correlation parallel to the diagonal in the $E_{\gamma_1} \times E_{\gamma_2}$ plane. This indicates that some rotational correlations survive even in the regime of strongly interacting bands, where the rotational damping phenomenon

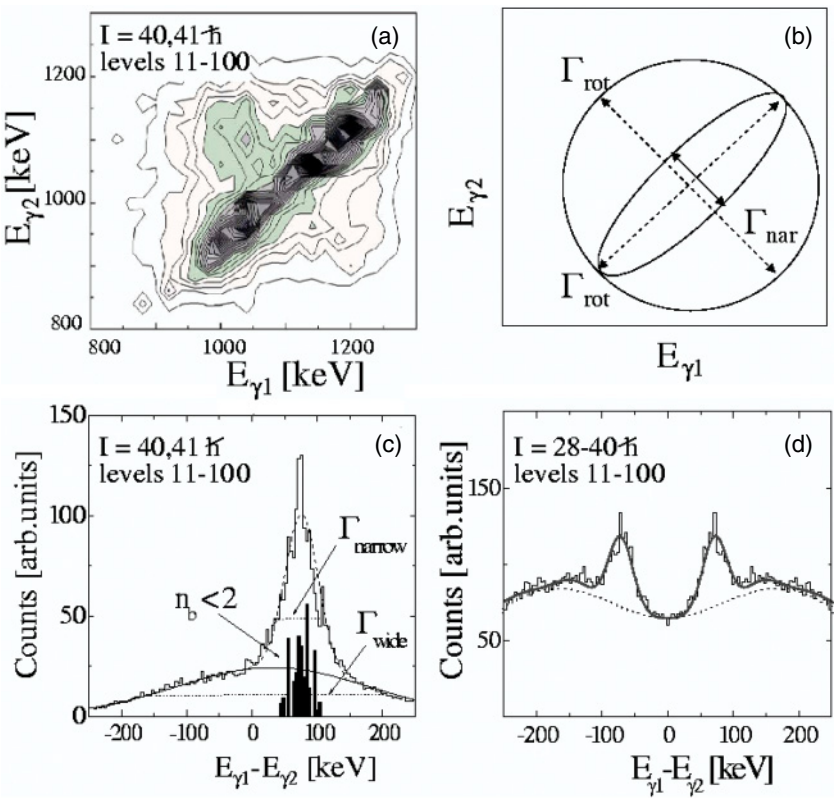

FIG. 11. (Color online) Illustration of the line-shape analysis technique applied and tested on simulated spectra. (a) An example of the calculated strength function for two consecutive $E2$ γ rays in the $E_{\gamma_1} \times E_{\gamma_2}$ plane. (b) Schematic of the analytic two-component function $S(E_{\gamma_1}, E_{\gamma_2})$, which is found to reproduce well the microscopically calculated $E2$ strength. (c) Projection on the E_{γ_1}-E_{γ_2} axis of the $E2$ strength shown in (a). In the figure, the full drawn line is the projection of the two-component Gaussian function schematically shown in panel (b), which contains wide and narrow distributions of width $\Gamma_{\rm wide} \approx \sqrt{2}\Gamma_{\rm rot}$ and $\Gamma_{\rm nar} \approx 2\Gamma_\mu$, respectively. The dark histogram represents the discrete bands distribution, which is obtained by requiring a branching number n_b smaller than 2. (d) A projection of a γ-γ spectrum calculated for several successive $E2$ decays. The full drawn line is the parametrization, which incorporates the two-component function, with $\Gamma_{\rm rot} = 180$ keV, $\Gamma_{\rm nar} = 44$ keV, and $I_{\rm nar} = 0.3$; the dashed line has no narrow component and a width $\Gamma_{\rm rot} = 150$ keV.

largely dominates. The $E2$ distribution of Fig. 11(a) can be well approximated by a two-component Gaussian function $S(E_{\gamma_1}, E_{\gamma_2})$ [illustrated in Fig. 11(b)], defined as

$$S(E_{\gamma_1}, E_{\gamma_2}) = I_{\rm nar} S^{\rm corr}(E_{\gamma_1}, E_{\gamma_2}) + (1-I_{\rm nar}) S^{I}(E_{\gamma_1}) S^{I-2}(E_{\gamma_2}), \quad (6)$$

where $S^{I}(E_{\gamma_1})$ $S^{I-2}(E_{\gamma_2})$ is the strength function for a single step decay from states at spin I (and $I-2$), which is a simple Gaussian function of FWHM $\Gamma_{\rm rot}$. In this way, the second term represents the uncorrelated part of the decay, giving rise to the wide component. The first term represents instead the narrow component $S^{\rm corr}(E_{\gamma_1}, E_{\gamma_2})$ of intensity $I_{\rm nar}$, which is correlated parallel to the diagonal line and has a narrow width in the E_{γ_1}-E_{γ_2} direction, as shown in Fig. 11(b). The $S^{\rm corr}(E_{\gamma_1}, E_{\gamma_2})$ distribution can then be parametrized by a two-dimensional Gaussian function characterized by the widths $\Gamma_{\rm nar}$ and $\Gamma_{\rm rot}$.

The two-component structure is even more evident in the projection of the $E2$ strength on the E_{γ_1}-E_{γ_2} axis, shown in Fig. 11(c). The projected $E2$ strength displays, in fact, a pronounced peak at the same position of the discrete band distribution, obtained by requiring that the branching number n_b of $E2$ branches out of a given state is less than 2 (dark histogram) [8]. As shown in the figure, the overall $E2$ distribution is well accounted for by the analytic function schematically illustrated in Fig. 11(b), made by the superposition of two Gaussians of width $\Gamma_{\rm wide}$ and $\Gamma_{\rm nar}$. As discussed in Ref. [26], it is found that the wide width $\Gamma_{\rm wide}$ is $\approx\sqrt{2}\Gamma_{\rm rot}$, whereas the narrow width $\Gamma_{\rm nar}$ is $\approx 2\Gamma_{\mu}$. This testifies to the fact that the narrow structure keeps memory of rotational correlation in the unperturbed *np-nh* shell model states, which at high excitation energies are smeared out by Γ_{μ}.

The two-component structure also determines the line shape of two- and higher fold quasicontinuum spectra, produced by several successive $E2$ γ decays [14]. This is seen in Fig. 11(d), which shows a projection of the calculated γ-γ spectrum, considering levels 11–100 only, for each I^{π}, in the spin range (28–40)$\hbar$ of ^{163}Er (neglecting the $E1$ contributions to the γ cascades). The calculations display a ridge-valley profile very similar to the experimental data, shown for example in Fig. 5, with a ridge structure at ± 70 keV that originates from the narrow component. Therefore, as discussed in Appendix B, a multidimensional strength function can be introduced to interpolate the experimental $E2$ spectrum, to extract directly the damping widths $\Gamma_{\rm rot}$ and Γ_{μ} and the intensity $I_{\rm nar}$ of the narrow component [cf. Eq (6)]. The strength function also depends on the number $N_{\rm step}$ of decay steps considered, which mostly determines the shape of the spectrum for rather large values of E_{γ_1}-E_{γ_2}. In such a procedure, the $J^{(2)}$ dynamic moment of inertia of the rotational states can be determined by the position of the two most inner ridges, as shown in Fig. 5. This is illustrated in Fig. 11(d), where the full drawn line is the parametrized 2D spectrum for several successive $E2$ steps, which incorporates the two-component function, with $\Gamma_{\rm rot} = 180$ keV, $\Gamma_{\rm nar} = 44$ keV, and $I_{\rm nar} = 0.3$. If one ignores the narrow component, as was previously done in Ref. [27], a simple Gaussian valley is obtained, as illustrated by the dashed line. This clearly indicates the importance of the narrow component for a proper reproduction of the overall spectrum line shape.

1. Test of the method on simulated spectra

The method has been tested on γ-γ coincidence spectra obtained by a Monte Carlo code that simulates the γ cascades via the competition between $E1$ and $E2$ transitions, at each step of the decay [23]. As discussed in detail in Appendix A, the simulation makes use of the levels and $E2$ transition probabilities microscopically calculated for the ^{163}Er nucleus [15]. Examples of 60-keV-wide cuts on the simulated matrices collecting the $E2$ strength from pure discrete rotational bands (bottom) and damped rotational states (top) are reported for comparison in the same panel in Figs. 12(a)–12(c). The projections are taken across the $E_{\gamma_1} = E_{\gamma_2}$ diagonal, at the average transition energies $\langle E_{\gamma}\rangle = 900$, 960, and 1020 keV, corresponding to spins $I = 30\hbar$, $32\hbar$, and $34\hbar$, respectively. In both cases the ridge-valley structure is clearly visible, with a separation between the two most inner ridges equal to $8\hbar^2/J^{(2)}$. Whereas in the discrete case the ridges are sharp (with a FWHM $\approx$ 20 keV) and strongly pronounced, a smoother pattern is observed in the damped spectra, with weaker and wider ridges and a central valley partially filled. The smooth lines superposed on the damped spectra are the best fit of the two-component spectral function previously discussed. The values obtained from the χ^2 minimization with respect to the intensity $I_{\rm nar}$ of the narrow component and to the parameter $N_{\rm step}$ are about 5% and 5 and are reported in the left-hand side of Table I; the results obtained for $\Gamma_{\rm nar}$ and $\Gamma_{\rm rot}$ are shown by stars in Fig. 12. The statistical errors associated with the four parameters $I_{\rm nar}$, $N_{\rm step}$, $\Gamma_{\rm rot}$ and $\Gamma_{\rm nar}$ cannot be evaluated from standard expressions, mainly because of the finite detector resolution (also included in the simulation), which implies that the counts in the different channels of the spectrum are not independent from each other. Instead, the evaluation can be obtained from the fluctuations in the number of counts in the spectrum [6]: The error Δa in the quantity a is determined by the value of Δa that satisfies the expression

$$\chi^2(a_0 \pm \Delta a) = \chi^2(a_0) + \frac{1}{n_{\rm ch}}\chi^2(a_0), \quad (7)$$

where a_0 is the best value obtained from the fitting procedure. In this expression $n_{\rm ch}$ indicates the number of channels in one dimension, which is equal to $\frac{4\hbar^2}{J^{(2)}}\frac{1}{R} = 60$ keV/4 keV $= 15$, where R is the channel resolution of the spectrum (typically 4 keV). The previous expression leads to rather small statistical errors (of the order of 5, 15, and 20% for $\Gamma_{\rm rot}$, $\Gamma_{\rm nar}$ and $I_{\rm nar}$, respectively), to which systematic errors, related to the uncertainties of the fit, have to be added, resulting in the error bars reported in Table I and Fig. 12. In particular, the fitting procedure is found to be rather sensitive to the energy range considered in the interpolation, which has always been applied at most to the interval $\pm 3 \times \frac{4\hbar^2}{J^{(2)}}$ around the valley region. In this way we are able to exclude regions of the spectra where the intensity rapidly decreases owing to the initial feeding conditions, which in the analytic function can only be partially accounted for by the $N_{\rm step}$ parameter.

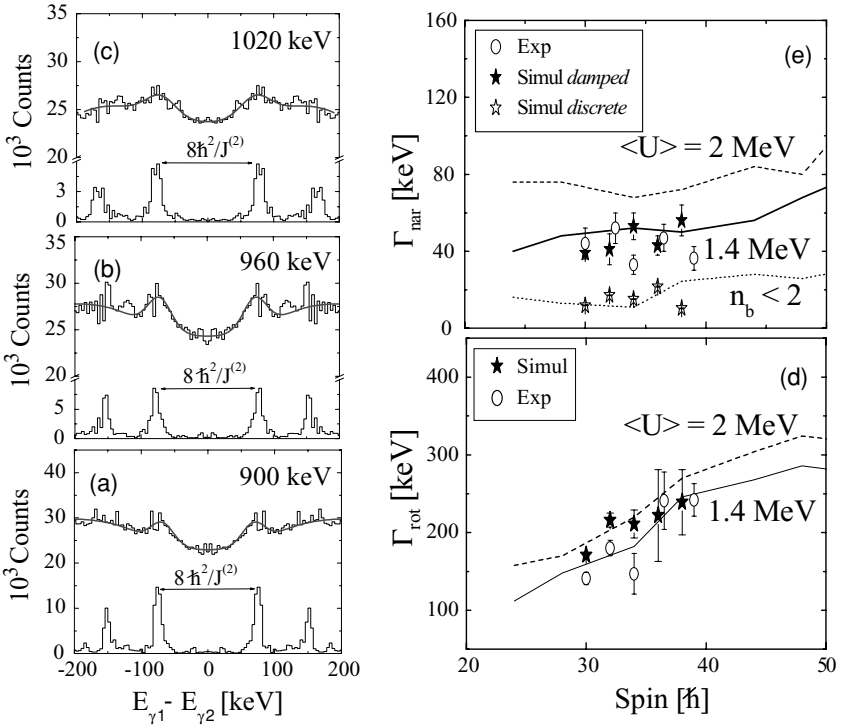

FIG. 12. Panels (a), (b) and (c) show 60-keV-wide projections on simulated spectra of ^{163}Er collecting the $E2$ strengths from discrete rotational bands (bottom spectra) and damped transitions (top spectra), at the average transition energies $\langle E_\gamma \rangle = 900$, 960, and 1020 keV. The interpolation of the damped spectrum by the two-component function is given by the solid line. Panels (d) and (e) show the calculated values of $\Gamma_{\rm rot}$ and $\Gamma_{\rm nar}$, respectively. The lines refer to the values calculated directly from the CSM bands at three different excitation energies: for $\langle U \rangle < 1$ MeV (in which case the bands branch out to less than two final states, $n_b < 2$), $\langle U \rangle \approx 1.4$ MeV, and $\langle U \rangle \approx 2$ MeV. The open (filled) stars refer to the values extracted from the simulated discrete (damped) spectra using the analytic parameterization. Finally, the open circles refer to the experimental data extracted from the spectra presented in Fig. 13.

The values of $\Gamma_{\rm rot}$ and $\Gamma_{\rm nar}$ obtained from the analysis of the simulated spectra are of the order of 200 and 40 keV, respectively, as shown in Figs. 12(d) and 12(e). The figure also shows the corresponding values deduced directly from the calculated CSM bands for the low-lying levels ($n_b < 2$), for the levels 11–100 [with $\langle U \rangle \approx 1.4$ MeV (solid line)], and for the levels 101–300 [with $\langle U \rangle \approx 2$ MeV (dashed line)], as discussed in Appendix B. It is found that the analysis of the simulated damped spectra agrees well in particular with the CSM prediction relative to the intermediate energy region, where the simulated γ-decay flow mostly goes at this spin interval. This clearly demonstrates the internal consistency of the present analysis technique.

2. *Experimental results*

The line-shape analysis technique has been applied to the *total*, *low-K*, and *high-K* experimental 2D spectra of ^{163}Er, discussed in Sec. II. After correcting for the detector efficiency, the pure $E2$ rotational correlations have been isolated by subtracting the $E1\times E1 + E1 \times E2 + E2 \times E1$ background contributions. The evaluation of the $E1$ component is obtained by assuming an exponential shape $\sim E_\gamma^3 \exp(-E_\gamma/T)$, where $T \approx 0.45$ MeV is the nuclear temperature [14,28].

Figure 13 shows examples of one-dimensional projections along the 60-keV-wide $E_{\gamma_1} = E_{\gamma_2}$ diagonal, at $\langle E_\gamma \rangle = 900$ and 960 keV (corresponding to spin $30\hbar$ and $32\hbar$). The projections are taken on the *total* matrix (panels a and b), and also on the *low-K* (panels c and d) and *high-K* (panels e and f) spectra. In all cases, one observes a rather smooth ridge-valley profile, very similar to the one displayed by the damped simulated spectra of fig. 12, apart from the ≈25% difference in the values of $J^{(2)}$. This results in a separation $8\hbar^2/J^{(2)}$ between the two most inner ridges of the order of 120 and 150 keV, respectively, for experimental data and simulation. The smooth curves in Fig. 13, well reproducing the experimental data, represent the best fits of the two-component spectral function.

In the right-hand side of Table I we give values for the parameters $I_{\rm nar}$ and $N_{\rm step}$ as obtained from the analysis of the *total* matrix. It is found that $N_{\rm step}$ is ≈5, whereas the intensity $I_{\rm nar}$ of the narrow component is in average ≈0.1, which is slightly higher than the simulated results. This can be partly attributed to some remaining contribution from discrete lines, which in the case of the experimental data are only removed according to the actual level schemes. As shown in Fig. 12, $\Gamma_{\rm rot}$ significantly increases in the spin region between $20\hbar$ to $60\hbar$, with values of the order of 200 keV, whereas the narrow width of the two-step distribution is more constant, providing values $\Gamma_\mu \approx 20$–30 keV over a wide spin region. In both cases good agreement is found with both the CSM predictions and the results from the simulated spectra.

TABLE I. Values obtained for the parameters $I_{\rm nar}$ and $N_{\rm step}$ by the χ^2 fitting of the parametrized spectrum applied to the simulated and experimental total matrix of ^{163}Er, as a function of spin.

Simulated			Experimental		
Spin [ħ]	$I_{\rm nar}$[%]	$N_{\rm step}$	Spin [ħ]	$I_{\rm nar}$[%]	$N_{\rm step}$
30	8 ± 2	6 ± 1	30	10 ± 2	5 ± 1
32	6 ± 1	6 ± 1	32	9 ± 2	5.5 ± 1
34	5 ± 2	5 ± 1	34	12 ± 2	6 ± 1
36	3 ± 1	4 ± 1	36	6 ± 2	6 ± 1
40	3 ± 2	4 ± 1	40	5 ± 1	5.7 ± 1

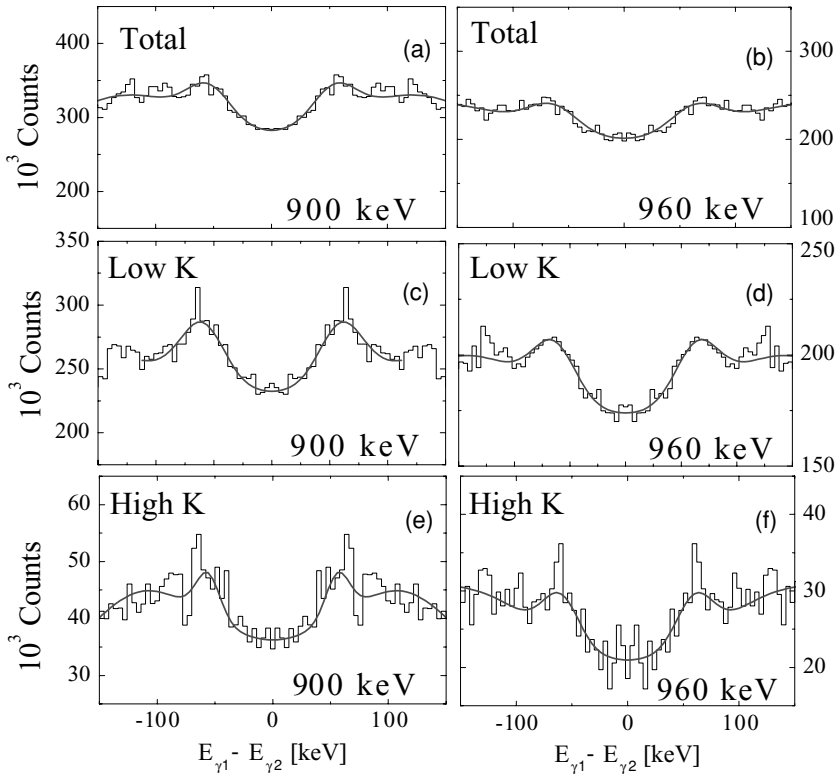

FIG. 13. 60-keV-wide projections on the E_{γ_1}-E_{γ_2} axis of experimental matrices of ^{163}Er, at the average transition energies $E_\gamma = 900$ and 960 keV. Panels (a) and (b) show projections on the *total* γ-γ matrix, whereas panels (c) and (d) and (e) and (f) correspond to spectra gated on *low-K* and *high-K* configurations of ^{163}Er. The (−150,150) keV interval shown here is equivalent to the one adopted in Figs. 12(a), 12(b), and 12(c) (namely (−200,200) keV), considering the different values of $8\hbar^2/J^{(2)}$ in the simulated and experimental spectra (≈150 and 120 keV, respectively).

The results from the analysis on the *low-K* and *high-K* matrices are shown instead in Fig. 14, in comparison with the corresponding low-K ($K \leqslant 8$) and high-K ($K > 8$) predictions from CSM calculations. In all cases the parameter $N_{\rm step} \approx 5$, while the intensity $I_{\rm nar}$ is in average 0.1 for *low-K* and 0.17 for *high-K*. The extracted values of $\Gamma_{\rm rot}$ and $\Gamma_{\rm nar}$ are in good agreement with the theoretical prediction relative to a colder decay flow (i.e. $\langle U \rangle \approx 1.4$ MeV), being, in average, of the order of 200 and 40 keV, respectively. A dependence of the damping width on the K values is also observed, since $\Gamma_{\rm rot}$ is almost 30% smaller for high-K states, as also shown in the calculations (see Appendix A for details). This points to a difference in the mixing process between low-K and high-K states, which can be related to a partial conservation of the K quantum number in the rotational damping region. This agrees both with the theoretical predictions, which show that high-K states maintain their rotational character even up to 1.5 MeV of excitation energies, namely in the region where rotational damping is otherwise largely dominating, and also with the experimental results from the variance and covariance analysis discussed in Sec. III A.

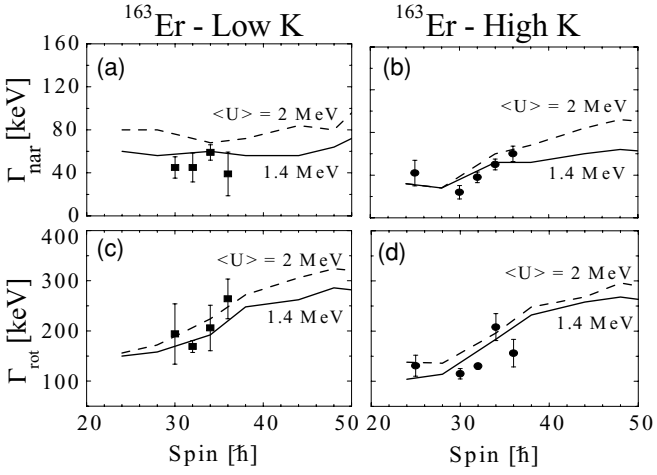

FIG. 14. Experimental values of $\Gamma_{\rm nar}$ and $\Gamma_{\rm rot}$, as extracted from the spectral shape analysis of experimental low-K (a and c) and high-K (b and d) γ-γ coincidence spectra of ^{163}Er. Predictions from CSM calculations [15] for average excitation energies of 1.4 and 2 MeV are shown by solid and dashed lines, respectively.

IV. CONCLUSIONS

We have here presented an extensive review of the experimental results obtained from the analysis of a high-statistics data set on the ^{163}Er nucleus. The analysis concerns the quasicontinuum γ-decay flow in the spin region (20–40) $\hbar$ and internal excitation energies up to around 2.5 MeV, where the transition between order and chaos is expected to take place. Two experimental techniques are discussed: (i) the statistical analysis of the fluctuations of counts in γ-γ matrices and (ii) the study of the line shape of quasicontinuum spectra. In both cases the data are sorted into γ-γ matrices in coincidence with specific intrinsic structures of ^{163}Er, which are characterized by small and large values of the K quantum number. The experimental results are compared with CSM calculations for this specific nucleus, providing a consistent picture for the overall description of the warm rotation at finite temperature, within the limitations of the theoretical framework.

By the use of the recently developed line-shape analysis technique, a direct experimental estimate of the rotational and compound damping widths $\Gamma_{\rm rot}$ and Γ_μ has been given, providing values of the order of $\approx$200 keV and $\approx$20 keV, respectively. Knowledge of the two damping widths can be viewed as a step forward in the understanding of the basic nuclear structure properties at finite temperature, since they both relate to the complex nature of the compound nucleus states.

In addition, a statistical analysis of the quasicontinuum spectra has allowed us to investigate the validity of the selection rules on the K quantum numbers with increasing internal excitation energy U, which can be used to investigate the order-to-chaos transition. It is found that, for internal energies below $\approx$1.2 MeV, the K quantum number is rather strictly conserved. However, at higher internal energy ($1.2 \leqslant U \leqslant 2.5$ MeV), the K quantum number is only partially conserved, pointing to a gradual transition toward a chaotic regime.

ACKNOWLEDGMENTS

The work has been supported by the Italian Institute of Nuclear Physics, by the Danish Natural Science Foundation Research Council, by the Polish Committee for Scientific Research (KBN Grant No. 2 P03B 118 22), by EU Transnational Access to Major Research Infrastructures (Contract No. HPRI-CT-1999-00078), and by the EU TMR project (Contract No. ERBFMRXCT970123).

APPENDIX A: MONTE CARLO SIMULATION OF THE γ-DECAY FLOW

The Monte Carlo code MONTESTELLA [4,23] can perform a simulation of the γ decay of the excited rotating nucleus from the residual entry distribution down to the yrast line. The simulation assumes that for well-deformed nuclei the γ decay is dominated by the competition between $E2$ collective and $E1$ statistical transitions [29]. The calculations produce simulated spectra of the same type of the experimental data, as shown, for example, in the right-hand side of Fig. 5, therefore providing a valuable tool for a quantitative study of quasicontinuum distributions.

The simulation makes use of energy levels and $E2$ transition probabilities microscopically calculated according to the model of Ref. [15], which is based on the cranking model and on the assumption of well-deformed nuclei with fixed deformation. In the model no pairing correlations are explicitly taken into account, therefore limiting the validity to the high-spin region of the γ decay. The use of calculated levels makes it possible, in particular, to perform a meaningful statistical analysis of the simulated γ-γ coincidence spectra, making use of the same analysis technique applied to the data [6] (see Sec. III). At excitation energies higher than the ones covered by the microscopic states (i.e., $U > 2.5$–3.0 MeV) it is assumed that the rotational decay proceeds through a continuum of states, governed by a rotational damping strength of Gaussian shape, with a width $\Gamma_{\rm rot}$ extrapolated from the region of the discrete, microscopically calculated levels. Also, the level density is extrapolated from the discrete region.

In the specific case of the ^{163}Er nucleus studied here, the microscopic levels used as input to the simulation code have been calculated by a recent version of the model that introduces in the Hamiltonian a J_z^2 term by taking into account the angular momentum carried by the K quantum number [15]. In the calculations, 4000 *np-nh* basis states of lowest excitation energy (corresponding to a cutoff of approximately 4 MeV) are used to diagonalize the Nilsson Hamiltonian with deformation parameters $\epsilon_2 = -0.252$ and $\epsilon_4 = -0.004$, for each I^π. The rotational bands are then mixed by the two-body residual interaction of surface delta type with standard interaction strength $V_0 = 27.5$ MeV/A. In this way, energy levels and $E2$ transition probability have been calculated in the spin range $I = (20$–$60)\,\hbar$, up to approximately 2.5–3 MeV above yrast. Every state is characterized by an intrinsic Gaussian distribution of K, with a FWHM σ_K that increase with U. Below $U \approx 1.5$ MeV, σ_K is found to be smaller than the typical spreading in the average value of K, so that it is possible to define two different sets of states (i.e., low K with $K \leqslant 8$ and high K with $K > 8$), which turn out to correspond to level densities differing by a factor of $\approx$3, as shown in Fig. 15. For $U \geqslant$ 2–2.5 MeV the average value of K converges toward $\langle K \rangle \approx 7$, thus explaining the rapid decrease in the number of high-K states observed in Fig. 15. In addition, since the intrinsic FWHM becomes larger than the spreading in the average values, the distinction between low-K and high-K configurations is blurred, corresponding to the statistical limit of strong K mixing. For energies around $U \approx 1.5$ MeV one finds an intermediate regime associated with the onset of K mixing.

In Fig. 16, we compare the experimental and calculated transition energies E_γ, as a function of spin I, for the four yrast bands A, B, E, and F of ^{163}Er. As one can see, good agreement is found between their average experimental value (solid line) and the calculated CSM values (filled diamonds), which are limited to the spin range (20–60) $\hbar$. This indicates that the average kinematic moment of inertia $J^{(1)}$ of the CSM bands is in good agreement with the experimental values, being $J^{(1)} = \hbar \frac{I}{\omega} = \hbar^2 \frac{I}{E_\gamma}$. A difference of $\approx$25% in the value

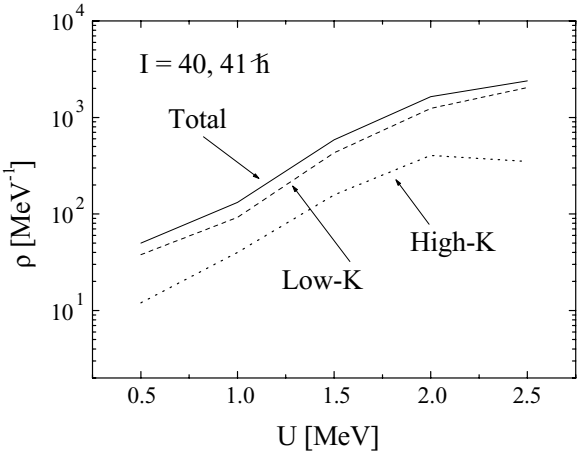

FIG. 15. The level density of ^{163}Er as a function of internal energy U at spin $I = 40\hbar, 41\hbar$, calculated according to the model of Ref. [15]. The solid line refers to the total number of states, the dashed (dotted) lines correspond to the states with $\langle K \rangle \leqslant 8$ ($\langle K \rangle > 8$).

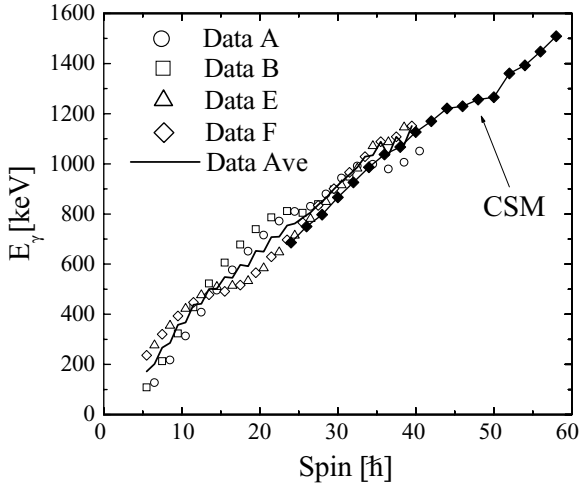

FIG. 16. The relation between the transition energy E_γ and the spin I, for the most intense experimental low-K bands (open symbols). The average among the experimental data (solid line) is also compared with the corresponding values from the CSM of Ref. [15] (filled diamonds).

of the dynamic moment of inertia $J^{(2)}$ is instead found between the experimental data and CSM bands, as can be seen from the separation $8\hbar^2/J^{(2)}$ between the two most inner ridges observed in γ-γ coincidence spectra (cf. Fig. 5), which gives values of the order of 120 and 150 keV, respectively.

In the previous version of the MONTESTELLA code [23] the total $E1$ transition probability is defined as

$$T(E1, U_i) = h_{E1} \int_0^{U_i} T(U_i, U_f) dU_f, \qquad \text{(A1)}$$

where

$$T(U_i, U_f) = (U_i - U_f)^3 f_{\mathrm{GDR}}(U_i - U_f) \frac{\rho(U_f)}{\rho(U_i)} \qquad \text{(A2)}$$

In this last expression $\rho(U_i)$ ($\rho(U_f)$) is the level density at the initial (final) excitation energy U_i (U_f) and f_{GDR} is the strength function given by the tail of the giant dipole resonance (GDR) of Lorentzian shape (assuming that the GDR exhausts the $E1$ sum rule), corresponding to a prolate nucleus with the same deformation parameters used to produce the microscopic bands. In the case of ^{163}Er, the centroid and width of the GDR are $E_0 = 15$ MeV and $\Gamma_{E1} = 5$ MeV, respectively. In the region of discrete levels, the previous integral is replaced by a summation.

It was generally found that, to reproduce the average experimental intensity of low-lying bands, one has to reduce substantially the value of f_{GDR} by introducing the hindrance factor $h_{E1} \approx 0.4$ [4,23]. This is illustrated in Fig. 17, where the fraction of the total intensity populating the ridge structure of ^{163}Er in the experimental γ-γ spectrum (symbols) is compared to the one of the simulated matrix, obtained by using hindrance factors $h_{E1} = 0.6$, 0.4, and 0.2.

In the present simulations we have also taken into account the microscopic structure of the quantum states connected by an $E1$ transition, multiplying $T(U_i, U_f)$ by an exponential quenching factor $P_{\Delta K}$ that takes into account the difference in

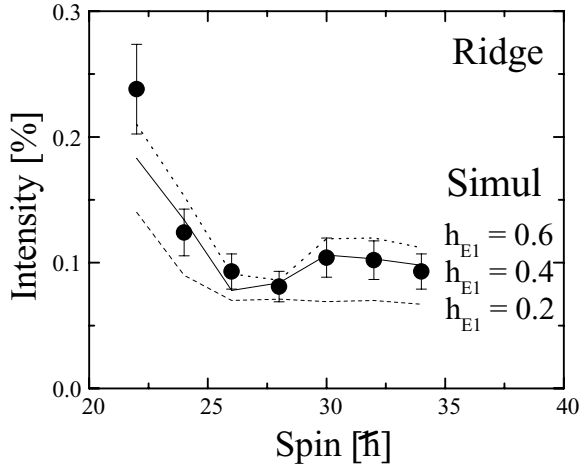

FIG. 17. Comparison of the fraction of the total intensity populating the ridge structure of ^{163}Er in the experimental γ-γ spectrum (symbols) and in the simulated matrix obtained using the hindrance factors $h_{E1} = 0.6$, 0.4, and 0.2.

the intrinsic K distribution. Such a factor is defined as

$$P_{\Delta K}(K_i, K_f) = C \int\int dk_1 dk_2 e^{-\frac{(k_1 - K_i)^2}{2\sigma_i^2}} e^{-\frac{(k_2 - K_f)^2}{2\sigma_f^2}} e^{-\frac{|K_f - K_i|}{\sigma}}, \qquad \text{(A3)}$$

where K_i (K_f) and σ_i (σ_f) are the average values and the standard deviations, respectively, of the K quantum number of the initial (final) state; the constant C is chosen to reproduce the average value of the total transition probability given by Eq. (A1), with $h_{E1} = 0.4$. The value of σ used in the $P_{\Delta K}$ expression of the ^{163}Er calculation is $\approx$0.3, in accordance with a standard estimate for K forbiddeness [3]. Such a value corresponds to a hindrance factor for degree of K forbiddeness of the order of 20, in agreement with the analysis of the $E1$ decay-out from isomeric states [30,31]. However, it turns out that our results are not very sensitive to the introduction of the factor $P_{\Delta K}$ in the calculations.

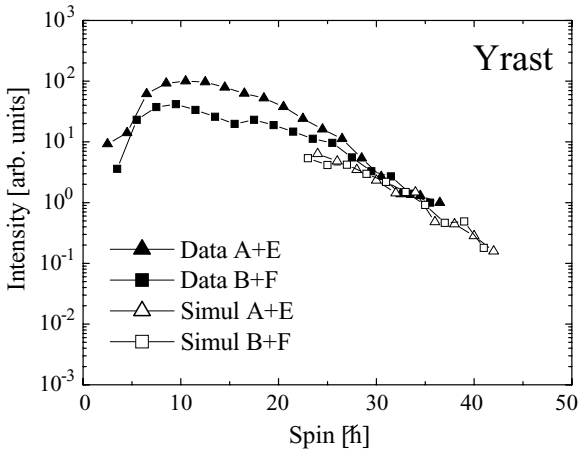

FIG. 18. Comparison of the measured and calculated intensities of the discrete γ transitions of the strongest populated bands in ^{163}Er as a function of spin, relative to the strongest yrast transition.

In the simulations the initial values of U and I for each γ cascade are selected from a Gaussian distribution with centroids and widths reproducing the experimental conditions. In the case of the ^{163}Er experiment, we have used $\langle U\rangle = 4$ MeV, $\mathrm{FWHM}_U = 4$ MeV and $\langle I\rangle = 44\ \hbar$, $\mathrm{FWHM}_I = 20\hbar$. The resulting simulated intensities reproduce well the experimental values both for ridge structures and low-spin yrast transitions, as illustrated in Figs. 17 and 18.

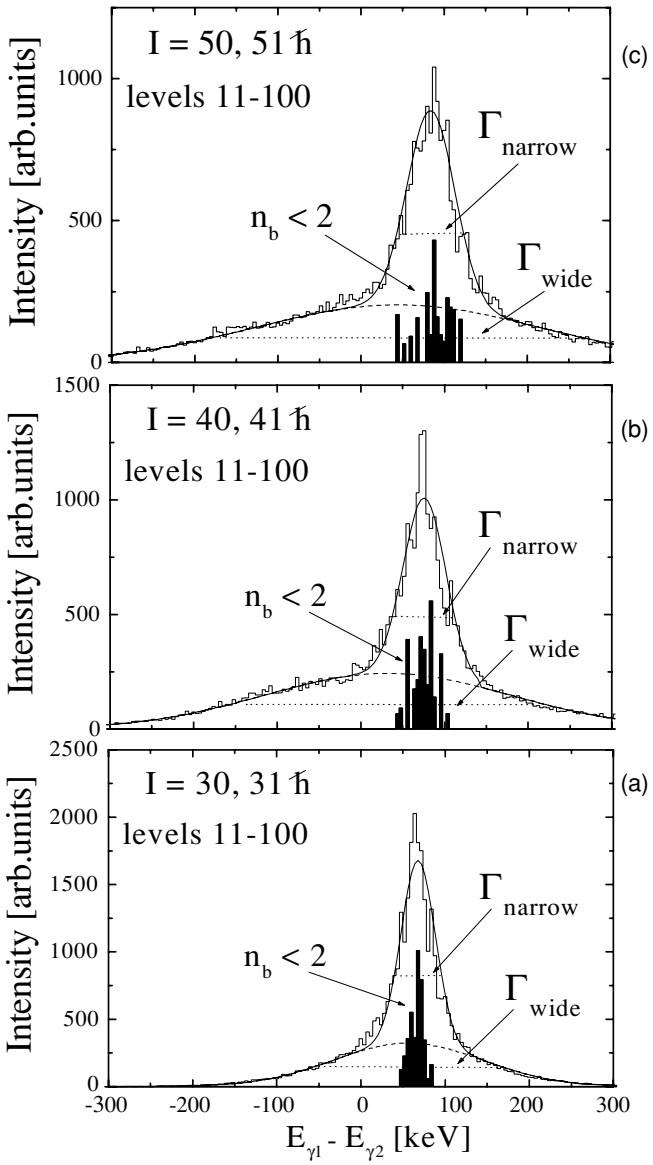

FIG. 19. Projections on the E_{γ_1}-E_{γ_2} axis of the strength function for two consecutive $E2$ γ rays, obtained by microscopic CSM calculations of ^{163}Er [8,12], for the levels 11 to 100 for each I^π. The calculations are performed at spin $I = 30\hbar$, $31\hbar$ (a), $I = 40\hbar$,$41\hbar$ (b), and $I = 50\hbar$,$51\hbar$ (c). The full drawn line is the two-component function, which contains wide and narrow Gaussian distributions of width $\Gamma_{\mathrm{wide}} \sim \sqrt{2}\Gamma_{\mathrm{rot}}$ and $\Gamma_{\mathrm{nar}} \sim 2\Gamma_\mu$, respectively. The discrete bands distribution (defined by the relation $n_b < 2$) is also shown by histograms.

APPENDIX B: ANALYSIS OF THE $E2$ STRENGTH FUNCTION

Direct information on the rotational and compound damping widths Γ_{rot} and Γ_μ can also be obtained from the microscopic model on which the Monte Carlo simulation is based (see Appendix A). In fact, as discussed in connection with the line-shape analysis presented in Sec. III B, the strength function for two consecutive $E2$ γ decays, $(I+2) \rightarrow I \rightarrow (I-2)$, characterizing the shape of the first ridge as well as the central valley in 2D γ-coincidence spectra, displays a two-component structure that can be related to the two different damping mechanisms (cf. Figs. 1 and 11) [26].

Figure 19 shows examples of projections of the $E2$ strength on the E_{γ_1}-E_{γ_2} axis, as obtained from calculations performed for levels 11–100 of ^{163}Er (corresponding to the average internal energy $\langle U\rangle \approx 1.4$ MeV), at spin values $I = 30\hbar$, $31\hbar$ (panel a), $I = 40\hbar$, $41\hbar$ (panel b), and $I = 50\hbar$, $51\hbar$ (panel c), for each I^π. As one can see, in all cases the projected $E2$ strength displays a pronounced peak at the same position of the discrete band distribution (dark histograms), thus indicating that in the calculated spectra some rotational correlations survive even in the regime of strongly interacting bands. As shown in the figure, the overall $E2$ distribution is well accounted for by the analytic function schematically illustrated in Fig. 11(b), made by the superposition of two Gaussians of width $\Gamma_{\mathrm{wide}} \approx \sqrt{2}\Gamma_{\mathrm{rot}}$ and $\Gamma_{\mathrm{nar}} \approx 2\Gamma_\mu$ (solid line in each panel of Fig. 19).

Interpolating the $E2$ strength distribution for two consecutive γ rays by a two-component Gaussian function, as shown in Fig. 19, one can extract the quantities Γ_{rot} and Γ_{nar} (hence Γ_μ) from the microscopic model, as a function of spin and internal excitation energy, as shown in Fig. 20. Although Γ_{rot} is found to

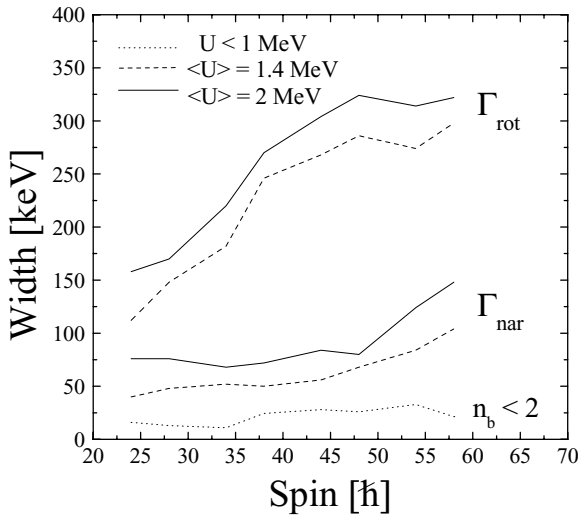

FIG. 20. Values of Γ_{rot} and Γ_{nar}, as a function of spin, extracted from the FWHM of the *wide* and *narrow* component of the two-step distribution shown in Fig. 19. The calculations are performed for the sets of levels 11 to 100 (dashed lines) and 101 to 300 (solid lines), corresponding to the average internal energy $\langle U\rangle \approx 1.4$ and 2 MeV, respectively. The dotted line gives the FWHM of the distribution of *discrete* bands (shown by histograms in Fig. 19 and defined by the condition $n_b < 2$).

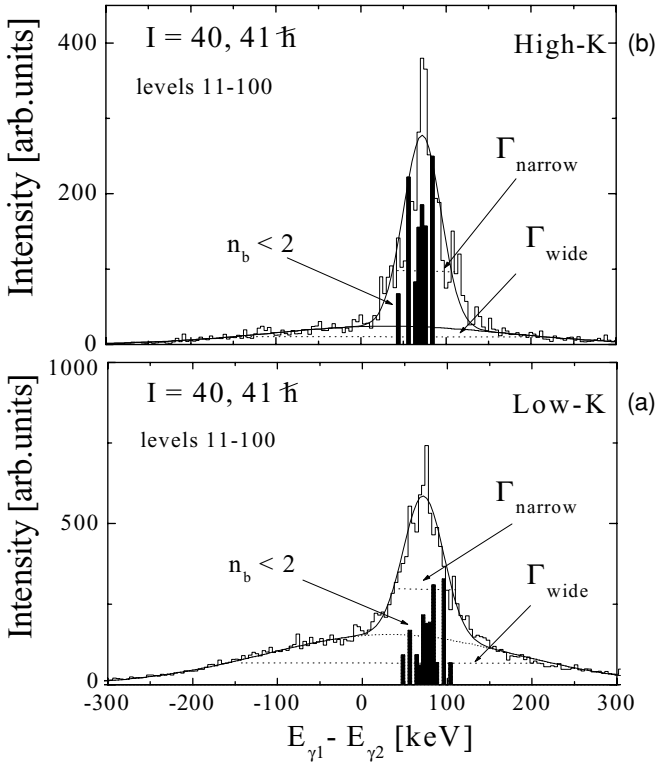

FIG. 21. The same as shown in Fig. 19 for (a) low-K ($K \leqslant 8$), and (b) high-K ($K > 8$) states, separately. In both cases, the calculated distribution is well accounted for by a two-component function containing wide and narrow Gaussian distributions of width $\Gamma_{\rm wide} \sim \sqrt{2}\Gamma_{\rm rot}$ and $\Gamma_{\rm nar} \sim 2\Gamma_{\mu}$, respectively. The discrete bands distribution (defined by the relation $n_b < 2$) is also shown by histograms.

significantly increase with spin in the region between $20\hbar$ and $60\hbar$, from ≈150 to 300 keV, the narrow width of the two-step distribution is more constant, providing values $\Gamma_{\mu} \approx 20$–30 keV over a wide spin region. In the figure we also show by a dotted line the FWHM of the discrete band distribution (represented by dark histograms in Fig. 19), which is found to be about half the width $\Gamma_{\rm nar}$ of the narrow component.

The dependence of $\Gamma_{\rm rot}$ and Γ_{μ} on the K quantum number can also be inferred by the analysis of the line shape of the two-step $E2$ strength, microscopically calculated. In fact, as shown in Fig. 21, the strength function, calculated separately for the low-K ($K \leqslant 8$) and the high-K ($K > 8$) levels 11–100, at spin $I = 40\hbar$,$41\hbar$, displays in both cases the distinct two-component structure. It is found that although Γ_{μ} depends only weakly on K, a 30% reduction is observed in the values of $\Gamma_{\rm rot}$ for high-K states, as shown in Fig. 14, in comparison with the data. This prediction is in good agreement with the experimental results discussed in Sec. III B.

The strength function for two consecutive $E2$ γ rays is reflected into the line shape of two- and higher-fold γ-coincidence spectra, which originate through several successive $E2$ decays. This results in the typical ridge-valley landscape observed in experiment and reproduced in simulations, shown for example in Figs. 5 and 11(d). Therefore, a multidimensional strength function $S(E_{\gamma_1}, E_{\gamma_2} \ldots E_{\gamma_n})$ can be introduced, leading to a parametrized spectral function for

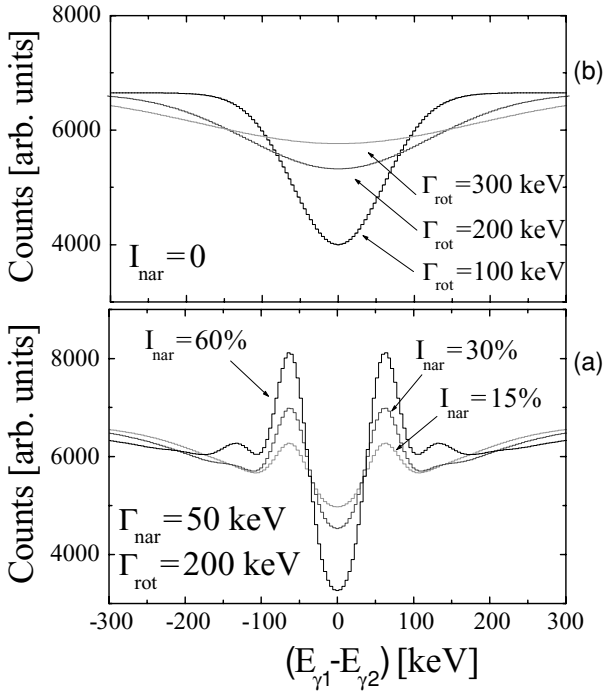

FIG. 22. (a) Projections of 2D parametrized spectra for several successive $E2$ decays. The calculations are performed for $I_{\rm nar} = 15$, 30, and 60%, assuming constant values for $\Gamma_{\rm nar} = 50$ keV and $\Gamma_{\rm rot} = 200$ keV. (b) Results obtained for different values of $\Gamma_{\rm rot}$ (i.e., 100, 200, and 300 keV), if no narrow component is included ($I_{\rm nar} = 0$).

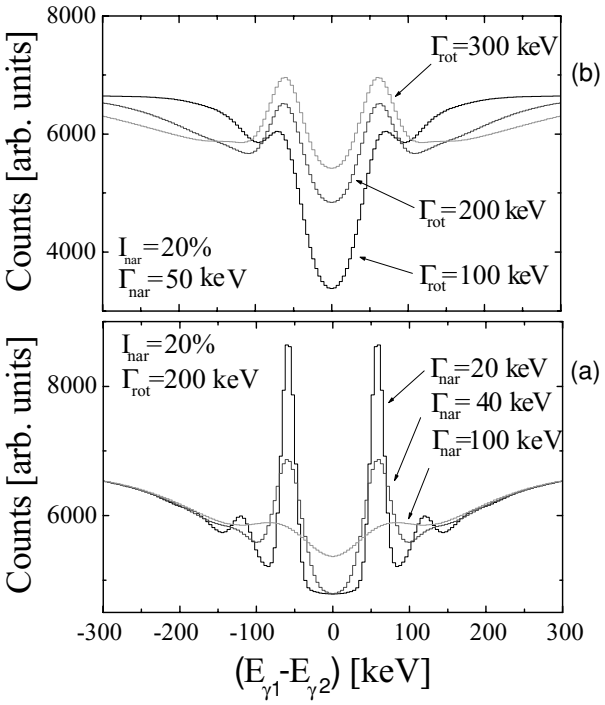

FIG. 23. Projections of 2D parametrized spectra for several successive $E2$ decays, obtained assuming a 20% constant value for $I_{\rm nar}$. In panel (a) the calculations are performed for $\Gamma_{\rm rot} = 200$ keV and $\Gamma_{\rm nar} = 20$, 40, and 100 keV. In panel (b) $\Gamma_{\rm nar}$ is 50 keV whereas the rotational damping width assumes the values $\Gamma_{\rm rot} = 100$, 200, and 300 keV, respectively.

2D (as well as higher order) γ-coincidence spectra. Such a function consists of the superpositions of many double-Gaussian distributions of width $\Gamma_{\rm rot}$ and Γ_μ, defined by Eq. (6), and it can be used to interpolate the line shape of experimental γ-coincidence spectra. In this way, values for the damping widths $\Gamma_{\rm rot}$ and Γ_μ, the intensity $I_{\rm nar}$ of the narrow component, and the number $N_{\rm step}$ of the decay steps considered can be extracted from the spectra. Figure 22(a) shows examples of projections, perpendicular to the $E_{\gamma_1} = E_{\gamma_2}$ axis, of parametrized functions for the γ-γ coincidence spectrum produced by several successive $E2$ decays. The calculations are done for $\Gamma_{\rm rot} = 200$ keV and $\Gamma_{\rm nar} = 50$ keV, and the intensity of the narrow component is $I_{\rm nar} = 15$, 30, and 60%, respectively. As one can see, not only does the analytic function display a ridge-valley structure similar to the one observed in the real data (cf. Fig. 5), but the overall line shape of the experimental spectrum is very sensitive to the presence of the narrow component. If one ignores the narrow component, as was previously done in Ref. [27], the $E_{\gamma_1} \times E_{\gamma_2}$ spectrum contains just one Gaussian valley, whose width depends only on $\Gamma_{\rm rot}$, as illustrated in Fig. 22(b). One can then conclude that the presence of the narrow component is crucial for a proper description of the line shape of actual γ-coincidence data and that a multidimensional fitting of the parametrized spectrum to the experimental $E2$ spectrum can make it possible to directly extract the damping and compound widths $\Gamma_{\rm rot}$ and Γ_μ from the data. In fact, as shown in Fig. 23, the spectral region including both the first ridge and the central $E_{\gamma_1} = E_{\gamma_2}$ valley turns out to be very sensitive not only to the intensity of the narrow component but also to the rotational and compound damping widths. The method has been applied to the analysis of high-K and low-K γ-γ coincidence data of ^{163}Er, discussed in Sec. III B.

[1] R. U. Haq, A. Pandey, and O. Bohigas, Phys. Rev. Lett. **48**, 1086 (1982).
[2] J. D. Garrett *et al*., Phys. Lett. **B392**, 24 (1997).
[3] A. Bohr and B. R. Mottelson, *Nuclear Structure, Volume II: Nuclear Deformations* (World Scientific, Singapore 1998).
[4] A. Bracco and S. Leoni, Rep. Prog. Phys. **65**, 299 (2002).
[5] S. Frattini *et al*., Phys. Rev. Lett. **81**, 2659 (1988).
[6] T. Døssing *et al*., Phys. Rep. **268**, 1 (1996).
[7] F. Stephens *et al*., Phys. Rev. Lett. **94**, 042501 (2005).
[8] M. Matsuo *et al*., Nucl. Phys. **A617**, 1 (1997).
[9] M. Matsuo *et al*., Nucl. Phys. **A620**, 296 (1997).
[10] S. Åberg, Phys. Rev. Lett. **64**, 3119 (1990).
[11] B. Lauritzen *et al*., Nucl. Phys. **A457**, 61 (1986).
[12] M. Matsuo *et al*., AIP Conf. Proc. **656**, 32 (2003).
[13] G. Benzoni *et al*., Phys. Lett. **B615**, 160 (2005).
[14] S. Leoni *et al*., Phys. Rev. Lett. **93**, 022501 (2004).
[15] M. Matsuo *et al*., Nucl. Phys. **A736**, 241 (2004).
[16] F. Stephens *et al*., Phys. Rev. Lett. **88**, 142501 (2002).
[17] S. Galès *et al*., Phys. Rev. C **18**, 2475 (1978).
[18] F. A. Beck, Prog. Part. Nucl. Phys. **28**, 443 (1992).
[19] J. Simpson, Z. Phys. A **358**, 139 (1997).
[20] G. B. Hagemann *et al*., Nucl. Phys. **A618**, 199 (1997).
[21] P. Bosetti *et al*., Phys. Rev. Lett. **76**, 1204 (1996).
[22] D. C. Radford, Nucl. Instrum. Methods A **361**, 297 (1995).
[23] A. Bracco *et al*., Phys. Rev. Lett. **76**, 4484 (1996).
[24] S. Leoni *et al*., Nucl. Phys. **A671**, 71 (2000).
[25] B. R. Mottelson, Nucl. Phys. **A557**, 717c (1993).
[26] M. Matsuo *et al*., Phys. Lett. **B465**, 1 (1999).
[27] S. Leoni *et al*., Nucl. Phys. **A587**, 513 (1995).
[28] S. H. Sie *et al*., Phys. Rev. Lett. **46**, 405 (1981).
[29] T. Døssing and E. Vigezzi, Nucl. Phys. **A587**, 13 (1995).
[30] P. Walker *et al*., Phys. Lett. **B408**, 42 (1997).
[31] F. G. Kondev *et al*., Nucl. Phys. **A632**, 473 (1998).